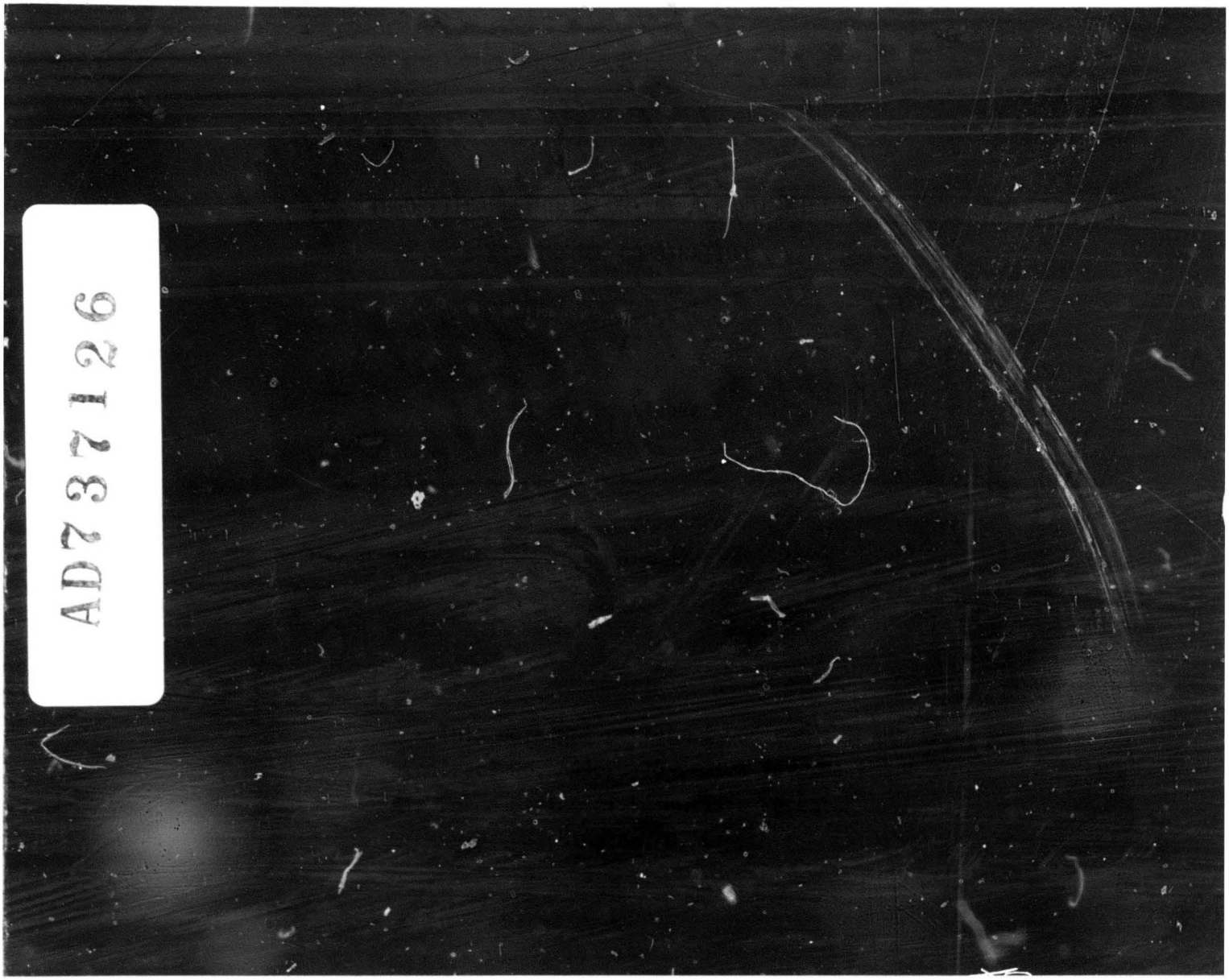

MCDONNELL DOUGLAS

UNCLASSIFIED
Security Classification

DOCUMENT CONTROL DATA - R & D

(Security classification of title, body of abstract and indexing annotation must be entered when the overall report is classified)

1. ORIGINATING ACTIVITY (Corporate author)

DOUGLAS AIRCRAFT COMPANY
McDONNELL DOUGLAS CORPORATION
3855 LAKEWOOD BLVD., LONG BEACH, CALIFORNIA 90801

2a. REPORT SECURITY CLASSIFICATION

UNCLASSIFIED

2b. GROUP

3. REPORT TITLE

THEORETICAL STUDIES ON THE AERODYNAMICS OF SLAT-AIRFOIL COMBINATIONS

4. DESCRIPTIVE NOTES (Type of report and inclusive dates)

Scientific Final

5. AUTHOR(S) (First name, middle initial, last name)

ROBERT H LIEBECK

6. REPORT DATE	7a. TOTAL NO. OF PAGES	7b. NO. OF REFS
28 May 1971	67	5

8a. CONTRACT OR GRANT NO		9a. ORIGINATOR'S REPORT NUMBER(S)
	F44620-70-C-0108	
b. PROJECT NO.	9781-02	MDC J5195
c.	61102F	9b. OTHER REPORT NO(S) (Any other numbers that may be assigned this report)
d.	681307	

10. DISTRIBUTION STATEMENT

Approved for public release; distribution unlimited.

11. SUPPLEMENTARY NOTES	12. SPONSORING MILITARY ACTIVITY
TECH, OTHER	AF Office of Scientific Research (NAM) 1400 Wilson Boulevard Arlington, Virginia 22209

13. ABSTRACT

This report describes the results of a theoretical study on the analysis and design of leading edge slat plus main airfoil combinations. Originally it was planned to approach this problem using three basic methods: I. Representation of the slat by a point vortex, II. Representation of the slat by a set of thin airfoil theory singularity distributions, and III. exact solution of the complete two element airfoil problem using conformal mapping methods. After developing the basic analytical work for method III, it became apparent that the remaining analysis and computer programming required for even a rudimentary evaluation of this approach would exceed the total time available for the entire study. Therefore, it was decided to concentrate on the development of Methods I and II. An "on-line" computer graphics program was prepared for the solution and evaluation of Method I. The main airfoil is chosen from an infinite set of airfoils whose mapping functions to the unit circle are analytically defined. (The classical Joukowski airfoils are members of this set.) The vortex strength and position with respect to the main airfoil is then prescribed and the program calculates and displays the velocity distribution on the airfoil with and without the vortex present. This program has been applied to the study and development of some basic slat design guidelines which are presented. The problem of designing a leading edge slat which provides a specified velocity modulation on the nose region of a main airfoil has been studied using the approach of Method II. A computer program has been prepared which for a given slat thickness distribution designs a slat camber line that provides a specified velocity modulation on the nose region of an ellipse. Sample results are included for a limited set of test cases.

DD FORM 1 NOV 68 1473

UNCLASSIFIED
Security Classification

14 KEY WORDS	LINK A		LINK B		LINK C	
	ROLE	WT	ROLE	WT	ROLE	WT
AERODYNAMICS						
AIRFOIL						
LEADING-EDGE SLAT						
MULTI-ELEMENT AIRFOIL						

THEORETICAL STUDIES ON THE AERODYNAMICS OF SLAT-AIRFOIL COMBINATIONS

by

Robert H. Liebeck

Report No. MDC J5195

28 May 1971

FINAL REPORT

This work was performed under
Contract No. F44620-70-C-0108 for the
Air Force Office of Scientific Research
Washington, D. C.

Copy number

Report number MDC J5195

THEORETICAL STUDIES ON THE AERODYNAMICS OF SLAT-AIRFOIL COMBINATIONS

Revision date

Revision letter

Issue date 28 May 1971

Contract number

Prepared by Robert H. Liebeck

Approved by:

J. L. Hess, Chief
Basic Research Group
for Aerodynamics

A. M. O. Smith
Chief Aerodynamics Engineer
Research

O. R. Dunn
Director of Aerodynamics

This work was performed under
Contract No. F44620-70-C-0108 for the
Air Force Office of Scientific Research
Washington, D. C.

DOUGLAS AIRCRAFT COMPANY

MCDONNELL DOUGLAS CORPORATION

1.0 ABSTRACT

This report describes the results of a theoretical study on the analysis and design of leading edge slat plus main airfoil combinations. Originally it was planned to approach this problem using three basic methods: I. Representation of the slat by a point vortex, II. Representation of the slat by a set of thin airfoil theory singularity distributions, and III. Exact solution of the complete two element airfoil problem using conformal mapping methods. After developing the basic analytical work for Method III, it became apparent that the remaining analysis and computer programming required for even a rudimentary evaluation of this approach would exceed the total time available for the entire study. Therefore, it was decided to concentrate on the development of Methods I and II.

An "on-line" computer graphics program was prepared for the solution and evaluation of Method I. The main airfoil is chosen from an infinite set of airfoils whose mapping functions to the unit circle are analytically defined. (The classical Joukowski airfoils are members of this set.) The vortex strength and position with respect to the main airfoil is then prescribed and the program calculates and displays the velocity distribution on the airfoil with and without the vortex present. This program has been applied to the study and development of some basic slat design guidelines which are presented in this report.

The problem of designing a leading edge slat which provides a specified velocity modulation on the nose region of a main airfoil has been studied using the approach of Method II. A computer program has been prepared which for a given slat thickness distribution designs a slat camber line that provides a specified velocity modulation on the nose region of an ellipse. Sample results are included for a limited set of test cases.

2.0 TABLE OF CONTENTS

3.0 LIST OF FIGURES

4.0 LIST OF SYMBOLS

a, b Major and minor semi-axes of the ellipse.

B_I, B_J Singularity distribution mode coefficient.

$c_n = a_n + i\, b_n$ Complex coefficient defined by equation (6).

c_3 Radius of circle in z-plane defined by $c_3 = (a + b)/2$.

c_7 Constant defined by $c_7 = a^2 - b^2$.

c_s Slat chord length.

C_L, C_{L_T}, C_{L_A}, C_{L_S}, ΔC_L, C_{D_A} Aerodynamic coefficients of pole airfoil and point vortex system, see page 14.

C_p Pressure coefficient.

$C_{p_{min}}$ Minimum value of C_p, (also called "pressure peak").

(f_2, f_1) Coordinates of slat midchord in the W-plane.

L Total number of matching stations.

$q = u - iv$ Complex velocity.

(r, θ) Polar coordinates.

$S = s + i\, t$ Complex variable in the slat centered half-plane.

t_s Maximum thickness of slat.

u_{Ji} Influence coefficient of the Jth-mode at the ith station.

u_{mf} Main flow velocity parallel to slat at slat midchord in the S-plane.

$w(x_{3i}) = w_i$ Specified modulating velocity on x_3 - axis.

$w_t(x_{3i})$ Slat thickness induced velocity on x_3 - axis.

$W = x_3 + i\, y_3$ Complex variable in the half-plane.

$z = x_2 + i\, y_2$ Complex variable in the circle-plane.

$Z = x_1 + i\, y_1$ Complex variable in the ellipse-plane.

α Airfoil angle of attack.

α_s Slat chord angle with respect to x_3-axis in the W-plane.

Γ_A Adjusting circulation on circular cylinder.

Γ_C Circulation on circular cylinder.

Γ_S Point vortex circulation.

δ_i Defined on page 29.

ϕ Defined on page 30.

$\zeta = r\, e^{i\theta}$ Complex variable defined by equation (7).

$(\,)_i$ Refers to the ith matching station.

$(\,)_I$, $(\,)_J$ Refers to the Ith or Jth mode.

5.0 INTRODUCTION

The designer of high lift systems for modern aircraft is faced with a severely over-constrained problem. The satisfaction of cruise configuration geometry together with structural and mechanical requirements quite often results in a high lift system which is less than optimum aerodynamically. An additional complication results from the fact that even if the structural and mechanical requirements were relaxed, the aerodynamic design of high lift systems is still quite empirical and heavily reliant on wind tunnel testing. It is the purpose of this study to attempt to increase the knowledge and understanding of one of the basic components of a high lift system, the leading edge slat.

A primary function of a leading edge slat is to suppress the leading edge pressure peak on the main airfoil when it is operated at high angles of attack, and thus avoid boundary separation and possible stalling of the main airfoil. Referring to figure 1, the circulation about the slat creates a counter velocity component in the nose region of the main airfoil which results in a reduction of the pressure peak.

Although simple in principle, the design of efficient and effective leading edge slats is a very complex problem. In fact, it is not particularly clear that a "best" slat design exists or can even be rationally defined. On the other hand, a slat which provides a desired $C_{L_{max}}$ capability while satisfying the mechanical and structural requirements is certainly a successful design solution. In this light, some characteristic aerodynamic slat design problems can be defined whose solutions should provide a significant advance in the understanding and design capability of leading edge slats. It was not intended that all of the following problems be approached and solved under the limited scope of the present study, however, they are briefly discussed here in order to provide perspective for the present work.

(a) <u>Design of a slat which separates from the leading edge of the main airfoil</u>.

This is probably the most common of the slat design problems, and also

the most difficult from the aerodynamicist's point of view. Here the main airfoil geometry is already specified and the designer is asked to separate a portion of the leading edge to form a slat as shown in figure 2. The upper surface geometry of the slat is fixed, and the lower surface of the slat and the slat and the nose of the main airfoil must be shaped so they will fit together when the slat is retracted as shown in figure 2. The resulting slat is then oriented with respect to the main airfoil to provide the desired performance.

(b) Design of a slat which provides a specified modulated pressure distribution on the nose region of a given main airfoil.

This problem is less constrained than problem (a) above. The slat geometry and orientation are left completely free and it is only required that the resulting slat provides the specified pressure modulation distribution on the nose of the main airfoil. In addition, the flow should not separate on the slat itself.

(c) Simultaneous design of both the slat and the main airfoil.

It is obvious that this problem requires at least some generalized constraints or performance goals to have any solution at all. However a capability in this area could provide solutions to more specific problems such as: "design a two element airfoil system which obtains the maximum possible lift without separation".

Problems (a), (b), and (c) above are of course not distinct, nor do they represent in themselves the entire spectrum of leading edge slat design problems. They do serve to illustrate the basic forms which such problems take on, and this suggests the types of analyses which are most suitable in attempting to obtain design solutions.

There exist several theoretical analysis methods which may be applied to the leading edge slat design and analysis problems just described. One of the most powerful and versatile methods for the analysis of a multi-element

airfoil system of specified geometry is the Douglas Neumann potential flow computer program (reference 1). This program provides exact solutions for the potential flow field (on and off the bodies) for multi-element airfoil systems of up to five elements, and therefore is an extremely valuable tool for evaluating and predicting the aerodynamic performance of leading edge slat designs. This type of solution is called "direct" in that it requires the airfoil and slat geometry as an input. It can be used as a design tool by examining the results for a particular geometry, and then adjusting the geometry and re-running the program until the desired performance is obtained. Unfortunately the determination of what geometry adjustments should be made requires considerable experience and intuition, and this procedure tends to be rather costly and time-consuming. However, this approach appears to be the best available for problem (a) above at this time.

An analytic procedure for iterating with direct solution results has been developed by Wilkinson in reference 2 for the design of multi-element airfoil systems. The pressure distributions on the upper surfaces of the airfoil elements are prescribed, and an initial geometry is specified. Wilkinson's iterative procedure then systematically modifies the camber distributions of the airfoil elements. The maximum thicknesses, thickness distributions, chord lengths, and gaps between airfoil elements are maintained at all stages as equal to the respective quantities on the initial geometry. The advantage of this type of method lies in the fact that if a final solution is obtained (i.e. it converges) it is exact. However, there is no guarantee that an arbitrarily input set of initial geometries and upper surface pressure distributions can be iterated to convergence. This method is useful for approaching the solution of problem (c) above.

O'Pray in reference 3 has developed a linearized solution for problem (b) which for a given slat chord, slat orientation, and slat thickness distribution, shapes the slat camber line to provide the specified pressure modulation distribution on the nose region of the main airfoil. It appears, in principle, that this method can be extended to obtain a partial solution to problem (a): namely, instead of specifying the slat thickness distribution, the slat upper surface shape could be specified.

In the present work, it was originally decided to study the problem of leading edge slat analysis and design using three basic approaches:

I. Simulation of the slat by a point vortex.

II. Simulation of the slat by a finite set of singularity distributions.

III. Exact solutions using conformal mapping methods.

The choice of these approaches was based on the following reasons. The point vortex simulation of a slat represents the simplest possible theoretical model, and its formulation is straightforward analytically. The resulting analysis can be used to demonstrate the basic effects of slat position and slat lift coefficient, and these results are quite useful in both developing a more thorough understanding of slat performance, and in guiding the development of the more complex studies of approaches II and III.

The representation of the slat by a set of distributed singularities in approach II may be considered as the next step up in complexity of the theoretical model. Here, thin airfoil theory is used to describe the slat and the flow field which it imposes on the main airfoil. The effects of slat chord length, camber, and thickness as well as position and slat lift coefficient can be studied independently since thin airfoil theory allows superposition. In principle, this should provide linearized solutions of problems (a) and (b) above.

Approach III is by far the most elegant and general of the theoretical models considered in this study. Since conformal mapping techniques are to be employed, the final analysis should provide solutions to both direct and inverse (given the pressure distribution, find the corresponding geometry) problems. Once developed, exact solutions to problems (a), (b), and (c) should be obtainable using this method.

The investigations into the exact solution of slat airfoil combinations, by mapping into an annular domain and the generation of special solutions by mapping two disjoint circles have been carried out to the point where it is

clear that both approaches are promising analytically and appear practical. However, the funding under this contract was not sufficient for further computer work to be undertaken to test these concepts fully, so that it was considered advisable to concentrate the limited effort on the approximate methods (I and II). Nevertheless it is strongly recommended that the exact techniques should be examined further.

The following sections describe the development of the analysis of approaches I and II. A limited set of sample problems have been studied and the results of these are presented and discussed.

6.0 POINT VORTEX MODEL

6.1 General Discussion

As discussed earlier, the representation of the slat by a point vortex is the simplest possible theoretical model for studying the leading edge slat plus airfoil problem. From an analytic standpoint, this model has a particular appeal since the complex potential function for the flow field about a circular cylinder with a point vortex located outside the cylinder can be expressed in a simple closed analytic form by using Milne-Thompson's circle theorem (reference 5).

The basic problem is described in figures 3 and 4 where figure 3 shows the flow about a circular cylinder with circulation Γ_C. Figure 4 shows the flow about the same cylinder with the addition of an external point vortex of strength Γ_S. Merely combining the complex potential functions for the flow about a cylinder and for a point vortex will not yield the proper solution. Instead, an image vortex of strength $-\Gamma_S$ must be placed inside the cylinder where its location is readily determined using the circle theorem. The image vortex changes the circulation about the cylinder which in turn moves the stagnation points on the cylinder. Addition of a second vortex Γ_A at the center of the cylinder will return one (but not both) of the stagnation points to its original position when the strength Γ_A is properly set. For this study, the location of the rear stagnation point is held fixed so that when the cylinder is mapped into an airfoil the Kutta condition is maintained. Therefore the complex potential for the flow about a cylinder with circulation plus an external vortex present can be written down in a simple closed analytic form. It consists of the sum of the complex potentials for the cylinder plus those of the external vortex, its image, and the circulation correcting vortex.

In addition to the classical Joukowski airfoil, there exists an infinite set of airfoil shapes whose mapping derivatives to a circle may also be described analytically. These airfoils are referred to as "pole airfoils" on the basis

of the singularities used to define their mapping derivatives. A particular airfoil is defined by selecting pole locations, orders, and strengths within the unit circle, e.g. the Joukowski airfoil is defined by a first-order pole plus a second-order pole located coincidently inside the circle. Altering their location and strength changes the camber and thickness of the resulting airfoil. A rigorous derivation and analysis of the pole airfoil theory together with the addition of the external point vortex is given in reference 4, and therefore only the application of this theory will be discussed here.

Since the entire flow field about a pole airfoil plus point vortex can be described in closed analytic form, the study of this model lends itself particularly well to computer graphics. In this light, a computer program using the IBM System 360 computer together with the IBM 2250 display unit was written which provides "on-line" solutions. Operation of the program is basically as follows:

(1) The strengths and locations of the poles which are to define the airfoil are specified in the circle plane as shown in figure 5. (The choice of the particular values used to obtain a desired airfoil is described in reference 4). Figure 5 is a replica of the actual display which appears on the IBM 2250 screen. The pole specification values are typed in on a keyboard. The initial vortex location and strength is also typed in.

(2) Next, a transfer is made to the airfoil plane shown in figure 6 (which is also a picture of the actual IBM 2250 display). The top figure shows the airfoil geometry and location of the point vortex. The lower figure gives the airfoil surface velocity distribution as a function of s, the arc length along the airfoil surface beginning at the lower surface trailing edge and proceeding clockwise around the airfoil to the upper surface trailing edge. Three velocity distributions are shown: that for the airfoil alone, that imposed on the airfoil by the point vortex, and the combined result which represents the flow about the airfoil in the presence of the vortex. All of these solutions are exact.

(3) The airfoil angle of attack and the vortex strength and location can be changed by merely keying in different values as desired. The results are immediately displayed on the IBM 2250 screen in the form of figure 6. At any time the display may be printed for later reference which is the source of figures 5 and 6.

(4) The aerodynamic coefficients and parameters listed in figure 6 are defined and related as follows:

ALPHA (α): Airfoil angle of attack as measured from the chord line.

CL (C_L): Lift coefficient of the airfoil alone at that angle of attack.

CL TOTL (C_{L_T}): Lift coefficient of the total system (airfoil plus vortex).

CL AIRF (C_{L_A}): Lift coefficient of the airfoil in the presence of the vortex.

DEL CL (ΔC_L): Specified increment of lift for the total system (airfoil plus vortex) over the lift of the airfoil alone, i.e.

$$C_{L_T} = C_L + \Delta C_L \qquad (1)$$

CD AIRF (C_{D_A}): Drag coefficient of the airfoil in the presence of the vortex. (Drag on the vortex is equal and opposite to that of the airfoil.)

RADIUS, THETAV (r_v, θ_v): Location of the vortex in the circle plane.

An effective "slat" lift coefficient is defined by

$$C_{L_S} = C_{L_T} - C_{L_A} \qquad (2)$$

All of the aerodynamic coefficients are based on the airfoil chord and the free stream velocity, V_∞. This is more or less standard in multi-element airfoil work, and allows convenient relations such as those given by equations (1) and (2).

The various lift coefficients are related by equations (1) and (2), and typical operation of the program is as follows. Setting the airfoil angle of attack sets C_L, and setting ΔC_L specifies C_{L_T} from equation (1) or vice versa - independent of the position of the vortex so long as it lies outside of the airfoil. Moving the vortex will change C_{L_S} and C_{L_A} but they will always satisfy equation (2). The actual relation of these lift coefficients is derived from a careful application of Blasius' theorem to the two-body problem, and this is thoroughly described in reference 4.

It should also be noted that there is no net drag force on the airfoil plus vortex system as far as potential flow is concerned, and C_{D_A} represents a mutual repelling force between the vortex and the airfoil. It is this force which causes leading edge slats to extend automatically when released from their retracted position.

A sample result is shown in figures 7a and 7b. Figure 7a shows the result of an arbitrary specification of the vortex location and strength. It can be seen that this results in a severe and unwanted velocity spike near the leading edge. Leaving ΔC_L fixed and adjusting the vortex position to obtain a smooth velocity modulation yields the result shown in figure 7b. It was found that it was quite easy to select the proper vortex location and strength in order to obtain a smooth velocity modulation. This represents one of the major features and justifications for employing the computer graphics capability.

The following section describes the application of the point vortex model to some representative problems of multi-element airfoil analysis and design.

6.2 Point Vortex Model; Results and Conclusions

The pole airfoil plus point vortex program has been used to examine a limited set of leading edge design and analysis problems. In addition to the technical information obtained, this study has demonstrated the value of the on-line computer graphics capability of the program for providing the engineer

with a basic intuition regarding leading edge slat performance. This same intuition could be obtained without using computer graphics, and instead running a variety of cases and then reducing the data to provide similar results. However, the efficiency and vividness provided by the graphics capability appears to justify its use.

The example problems which follow are intended to demonstrate the capability of the pole airfoil plus point vortex program and evaluate the point vortex as a theoretical model for a leading edge slat. They should not be regarded as a comprehensive study of all of the possible applications of the program. Many potentially interesting problems have been left unexplored - due primarily to the limited time available for this study.

A nine percent thick cambered Joukowski airfoil (see figure 6) was used as the main airfoil in most of the example problems which follow. This profile was felt to be a representative geometry for leading edge slat applications. Moderate variations in airfoil camber and thickness failed to produce any significant qualitative changes in the results. One possible exception was that if the airfoil was very thick ($\sim 20\%$), the effectiveness of the point vortex as a slat was not very good in that it was necessary to locate a strong vortex at a large distance from the airfoil in order to obtain a satisfactory modulation. On the other hand, leading edge slats are not typically employed on very thick airfoils because they are not needed. It is likely, however, that much useful information could be gained from a closer examination of the effects of main airfoil geometry, but unfortunately time did not permit this in the present study.

Example 1.

It is desired to obtain a lift coefficient of 3.0 from a given airfoil (in this case the 9% thick cambered Joukowski airfoil) with and without a leading edge slat, and study the possible justification for using the slat. This example will also show how two airfoils may be combined to develop a total C_L of 3.0.

First, the Joukowski airfoil was generated and its angle of attack adjusted to provide $C_L = 3.0$ ($\alpha = 20.8°$) with no vortex present (see figure 8a). Next, a vortex of very low strength ($\Delta C_L = 0.03$) was located near the leading edge to provide the "best" possible suppression of the pressure peak. Due to the presence of the vortex the total lift coefficient becomes

$$C_{L_T} = C_L + \Delta C_L = 3.0 + 0.03 = 3.03$$

and therefore the angle of attack was reduced to obtain $C_{L_T} = 3.0$, and the result is shown in figure 8b. The vortex strength was then increased to $\Delta C_L = 0.08$ and the above process repeated, each time adjusting the vortex position to obtain the best possible modulation of the airfoil's pressure peak - a qualitative judgement. Sample results are shown in figures 8b, 8c, and 8d. In each case the total lift coefficient is the same, $C_{L_T} = 3.0$. The variations of the force coefficients C_{L_T}, C_{L_A}, C_{L_S}, and C_L together with the pressure peak $C_{P_{min}}$ of the modulated distribution are plotted versus α in figure 9.

The range of applicability of these results to conventional slat-airfoil performance is limited by the following consideration. To a rather crude approximation, the total lift of a typical slat plus airfoil combination is usually divided between the two elements in proportion to their respective chords. Slat chords are rarely as much as 20% of the main airfoil chord, and a more common value is on the order of 10%. Referring to figure 9, 20% of $C_{L_T} = 3.0$ gives $C_{L_S} = 0.6$ and $C_{L_A} = 2.4$ which suggests the limit of applicability of these results to conventional slat designs.

An interesting cross-plot can be obtained form the results of figure 9. Assuming the the slat chord is equivalent to the percentage C_{L_S}/C_{L_T}, the data in figure 9 may be used to generate a plot of $C_{P_{min}}$ versus slat chord required to provide it, i.e., from figure 9 a slat chord of 10% implies $C_{L_S} = 0.10 \times C_{L_T} = 0.3$ which corresponds to $C_{P_{min}} = -9$ at $\alpha = 20.5°$. The result is shown in figure 10. This should not be

regarded as a precise analytic fact, but rather as a qualitative indication of the relation between $C_{p_{min}}$ and the slat chord required to obtain it. It can be seen that a slat chord on the order of 10% of the main airfoil chord provides a very substantial reduction in $C_{p_{min}}$. Increasing the slat chord beyond about 15% produces a relatively small reduction in $C_{p_{min}}$.

Example 2.

Here it is desired to increase C_{L_T} while holding $C_{p_{min}}$ on the airfoil to a specified value which might be set by separation criteria. Again, a 9% thick cambered Joukowski airfoil was used. First, the airfoil angle of attack was set so that $C_{p_{min}}$ reached the specified value with no vortex present. The angle of attack was then increased by a few degrees and the vortex strength and position adjusted so that $C_{p_{min}}$ was reduced to the specified value using the minimum possible vortex strength. This process was then repeated until the airfoil angle of attack reached 45° which is somewhat beyond the range of practical operation. Sample results are shown in figures 11a, 11b, and 11c. The resulting variations of the various lift coefficients are shown in figures 12 and 13 for specified values of $C_{p_{min}}$ of -8 and -12 respectively. Also shown is the implied slat chord based on the ratio C_{L_S}/C_{L_T} as in Example 1. Using this data, a cross plot of C_{L_T} versus the implied slat chord required to obtain it was made and is shown in figure 14 for both $C_{p_{min}} = -8$ and $C_{p_{min}} = -12$.

One of the cruder forms of boundary layer separation criteria says that the existence of attached flow is dependent on some maximum (numerical) value of $C_{p_{min}}$ which lies somewhere between -8 and -12. A pressure peak which is higher is likely to cause separation - possibly of the entire upper surface of the airfoil since the peak is located near the nose. Therefore, figures 12 and 13 may be regarded as demonstrating the ability of a slat to increase the $C_{L_{max}}$ of an airfoil. Alternatively, these results demonstrate the ability of a slat to increase the angle of attack range of an airfoil. Figure 14 shows that the slat chord required varies effectively linearly with the increase in C_{L_T}, and figures 12 and 13 show that the slat chord varies almost linearly with α.

Example 3.

The prescription of the strength and position of the vortex to obtain a "proper" or "best possible" modulation on the airfoil is, of course, to some extent subjective. However, it was found that if these parameters were set at the highest angle of attack at which the system was to be operated, when the angle of attack was reduced it was only necessary to reduce ΔC_L and not change the location of the vor : in order to obtain proper modulation at the lower angles. Conversely, if the vortex location was set at some intermediate angle of attack and proper modulation obtained there, it was invariably necessary to adjust both ΔC_L and the vortex position as the angle of attack was increased in order to provide a smooth modulation.

This phenomenon is illustrated by using the 9% thick Joukowski airfoil and requiring a very strong pressure modulation. The airfoil was set at $\alpha = 25°$ and ΔC_L and the vortex position (r, θ) were adjusted to obtain a smooth modulation as shown in figure 15a.

Reducing α to 20° but leaving ΔC_L, r, and θ fixed yielded the spiked pressure distribution shown in figure 15b. However, by simply reducing ΔC_L the smooth distribution shown in figure 15c was obtained. This process was continued down to $\alpha = -6°$, where at each interval ΔC_L was reduced just enough to obtain a smooth modulation and the vortex location remained fixed at the position set at $\alpha = 25°$. Some sample modulation distributions are shown in figures 16a, 16b, and 16c for $\alpha = 10°$, 5°, and 0°, respectively. The resulting variations in the lift coefficients versus α are shown in figure 17.

Figure 17 shows an almost linear variation of C_{L_T}, C_{L_A}, and C_{L_S} with respect to α. Since ΔC_L was set solely on the basis of the appearance of the resulting modulated pressure distribution this might not be an expected result. However, if the free stream velocity vector is considered as being made up of two components; $V_{\infty C}$ parallel to the chord,

and $V_{\infty N}$ normal to the chord, a simple explanation can be offered. For small α, $V_{\infty N}$ is nearly directly proportional to α, and it is the so-called "cross-flow component of velocity" $V_{\infty N}$ which causes the leading edge pressure peak on the airfoil. Therefore since $V_{\infty N}$ varies approximately linearly with α, and the intensity of the pressure peak does likewise, it is not surprising that the strength of the vortex required to suppress the peak also varies linearly with α.

The values of C_{L_S} which result are somewhat high for conventional slat applications. This is a consequence of the relatively strong modulation asked for initially which was used to illustrate the principles described above as vividly as possible. Also, the unmodulated pressure distributions at the lower angles of attack do not really require any modulation to avoid separation. However, as stated earlier, ΔC_L was reduced at each interval (value of α) just enough to remove any undesireable pressure spikes as shown in figure 15, and therefore some modulation remained - in fact, a negative ΔC_L was used at the lower angles of attack.

Example 4.

The purpose of this example was to test the validity of approximating a slat by a single point vortex. The geometry used was a 10% thick symmetrical Joukowski main airfoil with a cambered Joukowski airfoil whose chord was 10% of the main airfoil's for the slat. The slat was located in a typical position with respect to the main airfoil as shown in figure 18. The combination was then input into the Douglas Neumann potential flow program at an angle of attack of 15° which provided the aerodynamic coefficients of the system and its elements together with the pressure distributions on the elements.

Next, using the pole airfoil plus point vortex program, a point vortex was located at the slat quarter chord point and ΔC_L was set so that the total load on the vortex $\left(C_{L_S}{}^2 + C_{D_A}{}^2\right)^{1/2}$ was equal to the total load on the slat as calculated from the Douglas Neumann program results. The

resulting modulation distributions from both the point vortex and the slat are shown in figure 18, along with the values for C_{L_T} and C_{L_A}. The slat provides slightly more modulation than the vortex and thus the total lift of the slat plus airfoil system (C_{L_T} = 1.79) is less than that point vortex plus airfoil system (C_{L_T} = 1.84) for the same loading of the slat and point vortex.

Since the slat is positioned less than its chord length away from the nose of the airfoil, the above result is not surprising. It is expected that the distributed vorticity along the slat chord would provide more effective modulation than the concentrated vorticity of the point vortex. However, these results do demonstrate that using a point vortex to represent a slat as a first order theoretical model is a reasonable approach.

Example 5.

The point vortex can also be used to simulate a slotted flap at the airfoil trailing edge. An example of this is shown in figure 19 where the vortex is located just below the trailing edge. The circulation about the flap (point vortex here) causes an acceleration of the flow near the trailing edge on the main airfoil which reduces the pressure recovery requirement at the trailing edge. However, this also increases the velocity peak at the leading edge as can be seen in figure 19 which calls for a leading edge slat (or, in the present context, a second point vortex). At this time, the pole airfoil plus point vortex program does not have the capability for generating two independent point vortices, but it appears that this would be a logical next step in developing the program.

7.0 DISTRIBUTED SINGULARITY MODEL

7.1 General Discussion

As mentioned in the Introduction, a next level of sophistication beyond the point vortex model appears to be the representation of the slat by a continuous distribution of singularities along the slat chord. The use of thin airfoil theory for describing the slat and its effect on the main airfoil is particularly appealing from the standpoint that linearized theory allows the separation of camber and thickness, and moreover, the theory is quite simple and straightforward when compared with the exact solution formulation. Since, as discussed earlier, the exact goals of slat analysis and design theory are not completely clear, it is felt that a linearized analysis should be conducted in order to provide proper guidance for an exact solution study. It may be recalled that much of the fundamental information regarding the performance of single element airfoils comes directly from thin airfoil theory.

The basic "new" analytical problem of using thin airfoil theory to represent the slat is the determination of an appropriate system of imaging the slat singularity distributions so that the presence of the main airfoil is properly accounted for. At first, it appeared that an extension of the point vortex model to the case of distributed vorticity along a slat chord line might be the best approach to use. However, examination of the method developed by O'Pray in reference 4 suggested that continued development and evaluation of his work would probably be the most fruitful course to follow.

Since the available documentation of O'Pray's method was rather limited, it was first necessary to redevelop his entire analysis here at Douglas. Also, O'Pray obtained his sample solution using an on-line computer facility which allowed him to directly interact with the calculation procedure and adjust various inputs and parameters until a satisfactory result was obtained. Therefore it was decided to develop a new computer program which would minimize

if not eliminate any requirements for "man-in-the-loop" interaction. It is stressed that the above comments should in no way be interpreted as a criticism of O'Pray's work. Instead, his synthesis and formulation of the leading edge slat design problem was regarded as sufficiently impressive that further development was definitely in order. The discussion which follows is intended as a detailed description but not a rigorous development of O'Pray's method.

The problem to be solved is that of designing a leading edge slat which provides a specified pressure distribution modulation on the nose region of the main airfoil. As stated, this problem is somewhat underspecified and it is not likely to possess a unique solution. Therefore some additional conditions may be imposed. The use of thin airfoil theory implies representing the slat by an infinite set of singularity distributions whose coefficients are to be set on the basis of the boundary conditions which are to be satisfied. The pressure field imposed on the main airfoil by these singularity distributions is linear with respect to the magnitude of their coefficients and nonlinear with respect to the location of the slat chord. Thus it seems reasonable, at least to begin with, to specify the slat chord position, and then attempt to determine the proper values for the mode coefficients. The choice of the coefficients involves two basic requirements: (1) they must provide the desired pressure distribution modulation on the main airfoil, and (2) they must correspond to a real and useable geometry for the slat itself. (There is no a priori guarantee that an arbitrarily chosen set of mode coefficients might not imply a slat of negative thickness or one whose trailing edge does not close.)

One of the major features of O'Pray's method lies in the choice of the various conformal mappings employed. Instead of working with an arbitrary main airfoil shape, an ellipse of arbitrary thickness is used. It is observed that for most conventional airfoils without extreme leading edge camber or nose droop, the nose region itself is very nearly elliptical, and therefore the nose flow about an ellipse closely models the typical flow environment of a leading edge slat. Thus an ellipse with its circulation set to maintain the Kutta condition

at its trailing edge becomes a rather ideal model for a main airfoil to study slat performance since its mapping to a circle is straightforward.

7.2 Description of Analysis.

A. Mapping functions.

Several consecutive mappings are used in the analysis beginning with the mapping from the ellipse ($Z\ (x_1, y_1)$-plane, figure 20a) to the circle ($z\ (x_2, y_2)$-plane, figure 20b) where the mapping function is given by

$$\begin{aligned} Z &= z + c_7/4z \\ z &= {}^1/_2\left[Z + (Z^2 - c_7)^{1/2}\right] \end{aligned} \tag{3}$$

where $c_7 = a^2 - b^2$ and a and b are the major and minor axes of the ellipse. The radius c_3 of the corresponding circle in the z-plane is obtained from $c_3 = (a + b)/2$. Next, the circle is opened at its trailing edge and is mapped to the real axis of the half-plane ($W(x_3, y_3)$-plane, figure 20c) where $y_3 > 0$ corresponds to that region outside the circle. The point at infinity in the z-plane maps to $y_3 = 1$ in the W-plane, and the leading edge maps to the origin while the leading edge stagnation point maps to a small value of $- x_3$ on the negative real axis (if the angle of attack of the ellipse is zero, the stagnation point and the leading edge become coincident). The mapping from the circle-plane to the half-plane is

$$\begin{aligned} W &= i\left(\frac{z + c_3}{z - c_3}\right) \\ z &= c_3\left(\frac{W + i}{W - i}\right) \end{aligned} \tag{4}$$

The geom. ies of these mappings are shown in figure 20, where the modulation regi.. i: Indicated by the heavy line. Also shown in figure 20c are the streamlin.s o: .ne flow near the leading edge. It is observed that in the near vicinity of the modulation region the curvature of the streamlines is rather

moderate, and therefore a straight line slat chord may be placed tangent to one of the streamlines as shown in figure 20c. The selection of a particular slat chord position is based on the location, extent, and character of the desired modulation distribution. This will be discussed in greater detail later.

Once the slat chord position is set, a simple mapping to the slat-centered half-plane $\left(S\ (s,t)\ -\ \text{plane}\right)$ is made, where the origin of the S-plane lies at the slat midchord and the real axis parallels the slat chord as shown in Figure 20c. This mapping is merely a translation plus rotation plus dilation and is given by

$$S = \frac{4}{c_s}\, e^{i\alpha_s} \left[W - \left(f_2 + i f_1 \right) \right] \tag{5}$$

where f_2 and f_1 are the coordinates of the slat midchord, α_s is the slat angle with respect to the x_3-axis, and c_s is the slat chord length - all measured in the W -plane. Since it has been assumed that the slat chord will be set tangent to the local streamline which determines α_s, only the three parameters f_1, f_2, and c_s are needed to specify the slat. In the S-plane, the slat chord runs from $s = -2$ (the slat leading edge) to $s = +2$ (the slat trailing edge)*. This completes the mappings used in the analysis.

The main appeal of the above set of mappings lies in the fact that when a singularity distribution is defined on the slat chord, an identical singularity distribution may be defined on an image slat chord located as shown in figure 20c. This is the same procedure used for analyzing a conventional airfoil in ground effect where the ground surface becomes the axis of symmetry of the potential flow field. The fact that the main flow field in the W - plane is not a uniform stream does not affect this model. In the analysis which follows, the x_3 - axis of the W-plane (which is actually the surface

*A slat chord of 4 is convenient in defining the singularity distributions.

of the ellipse), will often be referred to as the "ground plane" in analogy to the above.

B. Singularity distributions.

The singularity distribution used to represent the velocity field induced by the slat comes from classical thin airfoil theory and has the form

$$q(\zeta) = \frac{c_0}{\zeta+1} + \sum_1^\infty \frac{c_n}{\zeta^n}, \qquad c_n = a_n + i\, b_n \tag{6}$$

where $q = u - iv$ is the complex velocity and ζ is related to the slat-plane variable S by the transformation

$$S = \zeta + 1/\zeta, \qquad \zeta = \frac{S + (S^2 - 4)^{1/2}}{2} \tag{7}$$

It should be noted that this is not a mapping function, but rather an independent variable transformation, i.e.,

$$q(S) = q\left[\zeta(S)\right]$$

and therefore in terms of S, equation (6) becomes

$$q(S) = \frac{c_0}{2}\left[1 - \left(\frac{S-2}{S+2}\right)^{1/2}\right] + \sum_1^\infty c_n \left[\frac{S - (S^2-4)^{1/2}}{2}\right]^n \tag{8}$$

The use of ζ as an independent variable is merely for convenience. Expanding the coefficients of equation (6) yields

$$q(\zeta) = \frac{a_0}{\zeta+1} + \sum_1^\infty \frac{a_n}{\zeta^n} + \frac{i\, b_0}{\zeta+1} + i \sum_1^\infty \frac{b_n}{\zeta^n}$$

where the a_n's represent slat thickness, and the b_n's represent slat camber. In order for the corresponding slat to close at its trailing edge the requirement

$$\lim_{\zeta \to \infty} \left[\frac{a_0}{\zeta + 1} + \sum_{1}^{\infty} \frac{a_n}{\zeta^n} \right] = 0$$

must be satisfied, which requires $a_0 + a_1 = 0$. For a finite nose radius $a_0 > 0$, and therefore a_1 is given by $a_1 = - a_0$.

In the case of the slat design problem considered here, the flow field imposed on the main airfoil by the slat will not be significantly affected by the higher order terms of the singularity distribution. Moreover, inclusion of a large number of terms in the least squares matching analysis (the discussion of which follows shortly) would tend to create numerical difficulties since the details carried by the higher order terms are not readily identifiable when one moves off the slat surface itself. Therefore the singularity distribution is defined as consisting of the first four thickness modes plus the first four camber modes. Since the first two thickness modes are coupled by the closure condition ($a_1 = -a_0$), the total number of independent modes is actually seven.

Using the form of equation (8) and redefining the a_n's and b_n's as B_I's, the seven singularity modes are defined as:

$$\left.\begin{aligned}
\tilde{q}_1(S) &= i \frac{B_1}{2} \left[1 - \left(\frac{S - 2}{S + 2} \right)^{1/2} \right] \\
\tilde{q}_2(S) &= i B_2 \left[\frac{S - (S^2 - 4)^{1/2}}{2} \right] \\
\tilde{q}_3(S) &= - i B_3 \left[\frac{S - (S^2 - 4)^{1/2}}{2} \right]^2 \\
\tilde{q}_4(S) &= i B_4 \left[\frac{S - (S^2 - 4)^{1/2}}{2} \right]^3
\end{aligned}\right\} \text{ camber modes} \qquad (9)$$

$$\left.\begin{aligned}
\tilde{q}_s(S) &= \frac{B_5}{2}\left\{\left[1-\left(\frac{S-2}{S+2}\right)^{1/2}\right]-\left[S-(S^2-4)^{1/2}\right]\right\} \\
\tilde{q}_6(S) &= -B_6\left[S-\frac{(S^2-4)^{1/2}}{2}\right]^2 \\
\tilde{q}_7(S) &= B_7\left[S-\frac{(S^2-4)^{1/2}}{2}\right]^3
\end{aligned}\right\} \text{thickness modes} \quad (9)$$

The corresponding slat geometry mode shapes are sketched in figure 21, and the velocity distribution of equation (6) becomes

$$q(S) = \sum_{I=1}^{7} \tilde{q}_I(S) = \sum_{I=1}^{7} B_I\, q_I(S)$$

in terms of S. The complex velocity in the half plane q (W) is given by

$$q(W) = q(S)\frac{dS}{dW} = q(S)\frac{4}{c_s}e^{i\alpha_s} \quad (10)$$

where dS/dW is obtained from equation (5). Now the real and imaginary parts of q(W) on $W = x_3$ ($y_3 = 0$) represent the parallel and normal slat singularity induced velocities on the ground plane (i.e. the ellipse surface in the W-plane). Defining

$$q_I(S) = u_I(S) - i\, v_I(S)$$

$$q_I(W) = u_I(W) - i\, v_I(W)$$

and using equation (10) yields

$$\begin{aligned}
u_I(W) &= \frac{4}{c_s}\left[u_I(S)\cos\alpha_s + v_I(S)\sin\alpha_s\right] \\
v_I(W) &= -\frac{4}{c_s}\left[u_I(S)\sin\alpha_s - v_I(S)\cos\alpha_s\right]
\end{aligned} \quad (11)$$

as the components of the velocity induced in the W-plane (half-plane) by each of the I singularity modes, where the $u_I(S)$ and $v_I(S)$ are known from the expressions given by equations (9).

Since an image slat is located in the lower half of the W-plane, the x_3-axis becomes an axis of symmetry, and on the x_3 - axis the total velocity induced by the slat plus image slat singularity distributions is simply

$$u(x_3) = 2 \sum_{I=1}^{7} B_I \, u_I \, (x_3) \tag{12}$$

where the $u_I(W)$ are defined by equations (11), and are functions of the slat chord and its position in the W-plane only. The factor 2 is due to the presence of the image slat.

C. Determination of the mode coefficients.

The problem remains to determine the coefficients B_I of the singularity distribution modes so that the induced velocity $u(x_3)$ provides the desired modulation on the ground plane (i.e. on the nose region of the ellipse). Typically the desired velocity modulation will be specified by a set of values at a finite number of discrete points along the ellipse nose surface. This specified velocity is readily mapped to the half-plane where it is defined as

$$w(x_{3i}) = w_i, \qquad i = 1, 2, ---, L \quad \text{(number of matching stations)}$$

where the x_{3i} are the matching stations. Next, comparing the desired velocity with that induced by the singularity distributions yields the L-equations

$$\delta_i = w(x_{3i}) - 2 \sum_{J=1}^{7} B_J \, u_J \, (x_{3i}), \quad i = 1, L$$

or

$$\delta_i = w_i - 2 \sum_{J=1}^{7} B_J \, u_{Ji}, \quad i = 1, L$$

The terms u_{Ji} are called "influence coefficients" and are defined as the velocity on the ground plane at the matching station x_{3i} induced by the Jth singularity mode with a unit mode coefficient.

The values of the mode coefficients B_J are determined using a standard least squares matching procedure. Letting

$$\phi = \sum_{i=1}^{L} \delta_i^2$$

and differentiating ϕ with respect to the B_J yields

$$\frac{\partial \phi}{\partial B_J} = \sum_{i=1}^{L} 2\,\delta_i \frac{\partial \delta_i}{\partial B_J} = 2 \sum_{i=1}^{L} \left(w_i - \sum_{J=1}^{7} B_J\, u_{Ji} \right) \left(- u_{Ji} \right) = 0$$

or

$$\sum_{i=1}^{L} u_{Ji}\, \delta_i = 0, \qquad J = 1, \text{---}, 7 \tag{13}$$

as seven simultaneous equations to be solved for the seven mode coefficients B_J. In matrix notation, equations (13) become

$$u\,(w - u^T B) = 0 \tag{14}$$

where the matrices of equation (14) are defined by

$u = \{ u_{Ji} \}$ = J x i rectangular matrix

$w = \{ w_i \}$ = i column matrix

$B = \{ B_J \}$ = J column matrix

Equation (14) can be rewritten in the form

$$u\,u^T B = u\,w$$

or

$$A\,B = C \qquad (15)$$

where $A = u\,u^T$, and $C = u\,w$. Equation (15) is a standard form and may be solved for B since A and C are known.

The resulting mode coefficients B_J provide the best possible fit by the singularity induced velocity distribution given by equation (12) to the specified modulation distribution $w(x_3)$. In principle, an arbitrarily large number of singularity modes could be used for this calculation, however it is likely that numerical instability would appear in the matrix inversion.

D. Corrections and adjustments to the mode coefficients.

Before proceeding to the determination of the slat shape corresponding to the mode coefficients B_J, it is necessary to consider some adjustments of the B_J which will improve the accuracy of the solution. These are the adjustment of the slat chord angle and a correction to the circulation about the ellipse.

It is recalled that the slat chord is initially positioned tangent to the local streamlines at midchord which in effect corresponds to a zero angle of attack in a uniform free stream. Referring to figure 21, the B_1 and B_3 camber modes serve to adjust the slat chord angle by increasing it when they are positive. It can be shown that the change in angle is given by

$$\Delta\alpha_s = \tan^{-1}\left(\frac{B_1}{2\,u_{mf}}\right) + \tan^{-1}\left(\frac{B_3}{3\,u_{mf}}\right) \qquad (16)$$

where u_{mf} is the local main flow velocity parallel to the slat at its midchord (V_∞ in a uniform free stream). It turns out that $\Delta\alpha_s$ is not necessarily small and therefore the initial slat chord angle should be adjusted

accordingly. This changes the values of the influence coefficients and therefore a repeat of the least squares solution is required to obtain a refined set of mode coefficients B_J. Repeating this procedure again is not justified on the basis of the inherent accuracy of thin airfoil theory.

Another correction arises due to the image slat vorticity. When mapped back to the ellipse plane, the image slat lies inside the ellipse and its vorticity due to the camber modes B_1, B_2, B_3, and B_4 moves the rear stagnation point and the Kutta condition is no longer satisfied. The image slat circulation is calculated by considering the problem in the circle plane. Most of the slat vorticity is contained in the B_1 and B_2 terms, and the B_3 and B_4 terms can be neglected within the accuracy of thin airfoil theory. The vorticity of the B_1 and B_2 terms is approximated by a point vortex of strength $2\pi B_1$ at the slat quarter chord and a point vortex of strength $2\pi B_2$ at the slat midchord. The corresponding image locations and circulation correction required to maintain the Kutta condition is then calculated in the circle plane using the same method as was employed in the point vortex model.

Even though the ellipse circulation correction amounts to less than one percent of the total ellipse circulation, it causes a significant change in the ellipse pressure distribution, particularly in the nose region. As a result the specified modulation velocity distribution $w(x_3)$ changes and therefore a new least squares solution is necessary. Due to the sensitivity of the nose flow to the ellipse circulation this procedure is repeated. Convergence to a negligible correction occurs after three or four cycles.

E. Slat thickness constraints.

Thus far in the analysis the calculation of the mode coefficients has been based almost solely on the requirement that they provide the desired velocity modulation distribution on the nose of the ellipse. It now becomes necessary to identify some geometrical considerations - in particular with respect to the slat thickness distribution. Earlier in the analysis closure of the slat was guaranteed by setting $a_1 = -a_0$. This does not, however, insure that the

thickness mode coefficients B_5, B_6, and B_7 as chosen by the least squares solution won't provide a slat thickness distribution which is re-entrant. In fact, it turns out that if the solution is left unconstrained this is quite often what happens. Such a result is readily understood when it is recalled that the slat is called on to provide a velocity modulation which opposes the main flow on the ellipse. This is accomplished by the circulation generated by the slat, however, in many cases positive thickness will tend to reduce this effect by causing an acceleration of the flow.

This difficulty is overcome by simply removing the thickness mode coefficients from the least squares matching solution, and prescribing them to provide any thickness distribution desired. The only modification required for the least squares solution is that the differences δ_i become

$$\delta_i = w(x_{3i}) - w_t(x_{3i}) - 2 \sum_{J=1}^{4} B_J \, u_J \, (x_{3i}), \quad i = 1, L$$

where $w_t(x_{3i})$ represents the velocity induced on the ground plane at x_{3i} by the prescribed slat thickness distribution, and of course there are only B_1, B_2, B_3, and B_4 (the camber mode coefficients) to be determined. It is convenient, but not necessary, to specify the thickness distribution by selecting values of B_5, B_6, and B_7, however any desired thickness distribution is in principle admissible.

For the examples worked in this study a basic thickness form made up of the B_5 and B_7 thickness modes was used. It can be shown that the B_5 mode coefficient is related to the maximum thickness (of that mode) by

$$B_5 = \frac{u_{mf} \, t_s}{0.65}$$

where u_{mf} is the local main flow velocity at the slat midchord and t_s is the maximum thickness to chord ratio. In order to thicken the back half of the slat, a negative B_7 mode coefficient was chosen whose magnitude was 20% of B_5, i.e.,

$$B_7 = -0.20 \, B_5$$

B_6 was set equal to zero.

The apparent necessity for prescribing the thickness distribution is not as bad as it may seem at first. In design problems, structural considerations often dictate thickness distribution requirements. The ability to specify the thickness distribution then allows an additional degree of freedom in the slat design problem since the camber distribution will then be calculated to provide the desired velocity modulation using the given thickness distribution.

F. Determination of slat geometry.

Once the camber mode coefficients B_1, B_2, B_3, and B_4 have been calculated, it remains to calculate the corresponding slat shape. Working in the S-plane, the standard flow tangency relation is

$$\frac{dt}{ds} = \frac{v}{u}$$

which upon integration gives

$$t(s) = \int_{+2}^{s} \frac{dt}{ds}\, ds = \int_{+2}^{s} \frac{v}{u}\, ds$$

where t is the slat surface ordinate. The integration is begun at the slat trailing edge ($s = +2$), and procedes forward (on the slat) to the slat leading edge ($s = -2$).

This integral is more easily evaluated if the transformation given by equation (7) is used which gives on the unit circle

$$s = 2\cos\theta, \qquad ds = -2\sin\theta\, d\theta, \qquad (\zeta = e^{i\theta})$$

and hence the integral takes the form

$$t(s) = -2\int_{0}^{\theta} \frac{v}{u}(\theta)\sin\theta\, d\theta$$

This is simplified to

$$t(s) = -\frac{2}{u}\int_0^{\theta} v(\theta)\sin\theta\, d\theta \qquad (17)$$

using the standard thin airfoil theory approximation that u is constant over the slat chord.

The normal velocity distribution along the slat chord $v(\theta)$ is made up of three basic contributions: $v_s(\theta)$ due to the singularity distributions on the slat chord, $v_{im}(\theta)$ due to the image slat, and $v_m(\theta)$ due to the main flow. More specifically, $v_s(\theta)$ is the imaginary part of $q(\zeta)$ or $q(S)$, and using equations (9) it has the form

$$v_s(\theta) = -\frac{1}{2}B_1 - B_2\cos\theta + B_3\cos 2\theta - B_4\cos 3\theta$$
$$\pm\left[B_5\left(\frac{1}{2}\tan\frac{\theta}{2} - \sin\theta\right) - B_6\sin 2\theta + B_7\sin 3\theta\right]$$

where for the bracketed terms, the (+) applies to the upper surface of the slat and the (–) applies to the lower surface. When substituted into equation (17), $v_s(\theta)$ can be integrated in closed form.

The distribution $v_{im}(\theta)$ represents the normal velocity induced at the slat by the singularity distributions on the image slat. $v_m(\theta)$ is the normal velocity distribution along the slat chord due to the fact that the main flow streamlines in the slat-plane are actually curved. If this were not included, the calculated slat shape would be erroneously cambered by an amount equivalent to the streamline curvature. Both $v_{im}(\theta)$ and $v_m(\theta)$ must be integrated numerically in equation (17).

Once the geometry solution $t(s)$ is obtained, it is mapped back to the ellipse plane using the mapping functions of equations (5), (4), and (3).

G. Method of calculation.

In order to evaluate the inverse slat design method just described, a computer program was written in Fortran IV language for the IBM System 360 computer. The required input data includes: the ellipse thickness ratio, the ellipse angle of attack, the desired pressure modulation distribution, the thickness distribution of the slat, the slat chord length c_s, and the slat midchord location (f_2, f_1). The program selects the proper slat chord angle α_s and determines the camber mode coefficients B_1, B_2, B_3, and B_4 which provide the closest possible match to the desired pressure modulation distribution. These calculations include the corrections for image induced circulation on the ellipse and slat chord angle. The resulting singularity distributions are then integrated to obtain the slat geometry including the necessary adjustments for the presence of the image slat and streamline curvature in the W-plane. Finally, the resulting geometry is mapped back to the ellipse plane to yield the actual slat shape.

In its present form, the program requires that the desired modulation distribution be input as a function of the Z-plane variable x_1, and of course the input variables c_s, f_1, and f_2 are defined in terms of W-plane coordinates. This was done for the sake of expediency in order to be able to evaluate the distributed singularity distribution model in the limited time available. As a consequence, prescribing this input data is somewhat more awkward than would be desirable - particularly for an individual with limited experience. However, once this data has been specified, the calculation of the slat geometry is completely automatic and requires no interaction with a "man-in-the-loop". The computer time required for a complete run on a 360/65 computer is less than one tenth of a minute, and therefore iterating to obtain a desired slat geometry is quite economical.

It should be noted that the program always yields a slat shape. However, if inappropriate values of c_s, f_1, or f_2 are specified, or an "impossible"

modulation is sought, the resulting slat geometry will likely be rather peculiar, and its modulation distribution may not completely agree with the one requested. Some sample results are presented in the following section.

7.3 Distributed Singularity Model: Results and Conclusions

The O'Pray inverse slat design method has been applied to a limited set of examples using the computer program developed in this study. These examples are intended to illustrate the basic viability of the method, and should not be regarded as a comprehensive display of all possible applications.

The main airfoil ellipse used for all of the examples is that chosen by O'Pray for his single test case: a 14% thick ellipse which in turn has a nose radius of about one percent of its chord. The ellipse is set at an angle of attack of about 17.2° (actually 0.3 radians) which gives a lift coefficient of 2.12, and a leading edge pressure peak of $C_{p_{min}} = -22.7$. A pressure distribution modulation is specified which reduces this pressure peak to $C_{p_{min}} = -9$. Figure 22 shows the pressure distribution on the nose region of the ellipse without modulation and that which results from the specified modulation distribution. (The other data shown in this figure will be explained shortly.) This pressure peak and required modulation of it are quite severe, and thus should represent a good test for the method.

The first problem considered was similar to O'Pray's test case: design a 10% thick slat to provide the specified modulation. Using the basic thickness distribution described in section 7.2E with $t_s = 0.10$, the slat shown in figure 23a was obtained. This slat geometry plus the ellipse was input into the Douglas Neumann potential flow program and the modulated pressure distribution provided by the slat is plotted in figure 22. The resulting slat geometry does not quite agree with that obtained by O'Pray, however, this result is not unexpected since his calculation routine was not the same as that of the Douglas program.

Next, the slat thickness was increased to 15% by setting $t_s = 0.15$, and to 20% by setting $t_s = 0.20$. The resulting slat geometrics are shown in figures 23b and 23c, respectively, and the resulting modulated pressure distributions as obtained from the Douglas Neumann program are shown in figure 22.

Finally, the ellipse angle of attack was increased to $\alpha = 18.4°$ (0.32 radians) which gives a lift coefficient of 2.3 ($Cp_{min} = -25.7$), and the same modulation ($Cp_{min} = -9$) requested. A 15% thick slat was called for and its resulting geometry is shown in figure 23d with the Douglas Neumann calculation of its corresponding modulated pressure distribution again plotted in figure 22.

The results shown in figures 22 and 23 indicate that there is no unique solution to problem (b) as described in the Introduction, and thus there exists a wide variety of slat geometries capable of accurately matching a specified pressure modulation distribution on the nose region of a given airfoil. This means that some of the slat geometry parameters (e.g. the thickness distribution) may be used to satisfy other constraints. These include structural, mechanical, and aerodynamic considerations. For example, it appears that it should be possible to constrain the upper surface shape of the slat, and with a proper reformulation of the method obtain solutions to problem (a) described in the Introduction. Similarly, it is possible that the method could be extended to handle the design problem where the upper surface velocity distribution would be constrained to avoid boundary layer separation on the slat itself. Unfortunately, the limited time available for this study did not permit such further investigations.

On the basis of the limited application and results obtained, the distributed singularity model as developed by O'Pray in reference 3 appears to be a practical slat design tool. At this time the method is still somewhat embryonic and requires some further refinement before it can be considered operational. This would include the ability to input arbitrary main airfoil geometries and their pressure modulations in the physical plane.

Operation of the present program is straightforward once one becomes used to working in the W-plane. The selection of the proper values of c_s, f_1, and f_2, is based on the character and location of the modulation distribution in the W-plane. A poorly chosen value for one of these parameters will usually provide a reasonable match of the modulation distribution, however, the resulting slat geometry may be unacceptable. For example, a value of c_s which is too small will result in a slat which is highly cambered at both ends (i.e. a large value of B_4) since this will tend to broaden the induced field. The value of f_2 will tend to shift the camber from one end to the other of the slat. In general, it has been found that by examining the agreement of the modulation distributions together with the values of the mode coefficients, an acceptable slat design can be obtained in less than five iterations. Since the total run time for the program on an IBM System 360/65 computer is less than 0.10 min., this procedure is quite economical.

8.0 REFERENCES

1. Hess, J. L., and Smith, A. M. O.: Calculation of Potential Flow About Arbitrary Bodies. Progress in Aeronautical Sciences, Vol. 8 (D. Kucheman, Ed.), Pergamon Press, New York, 1966.

2. Wilkinson, D. H.: A Numerical Solution of the Analysis and Design Problems for the Flow Past One or More Aerofoils or Cascades. R & M No. 3545, 1968.

3. O'Pray, J. E.: A Semi-Inverse Design Technique for Leading-Edge Slats. M.S. Thesis, California Institute of Technology, 1970. (To be published in the AIAA Journ. of Aircraft).

4. James, R. M.: A General Class of Airfoils Conformally Mapped from Circles. Douglas Report No. MDC J5108, May 1971.

5. Milne-Thompson, L. M.: Theoretical Hydrodynamics, MacMillan, 1950.

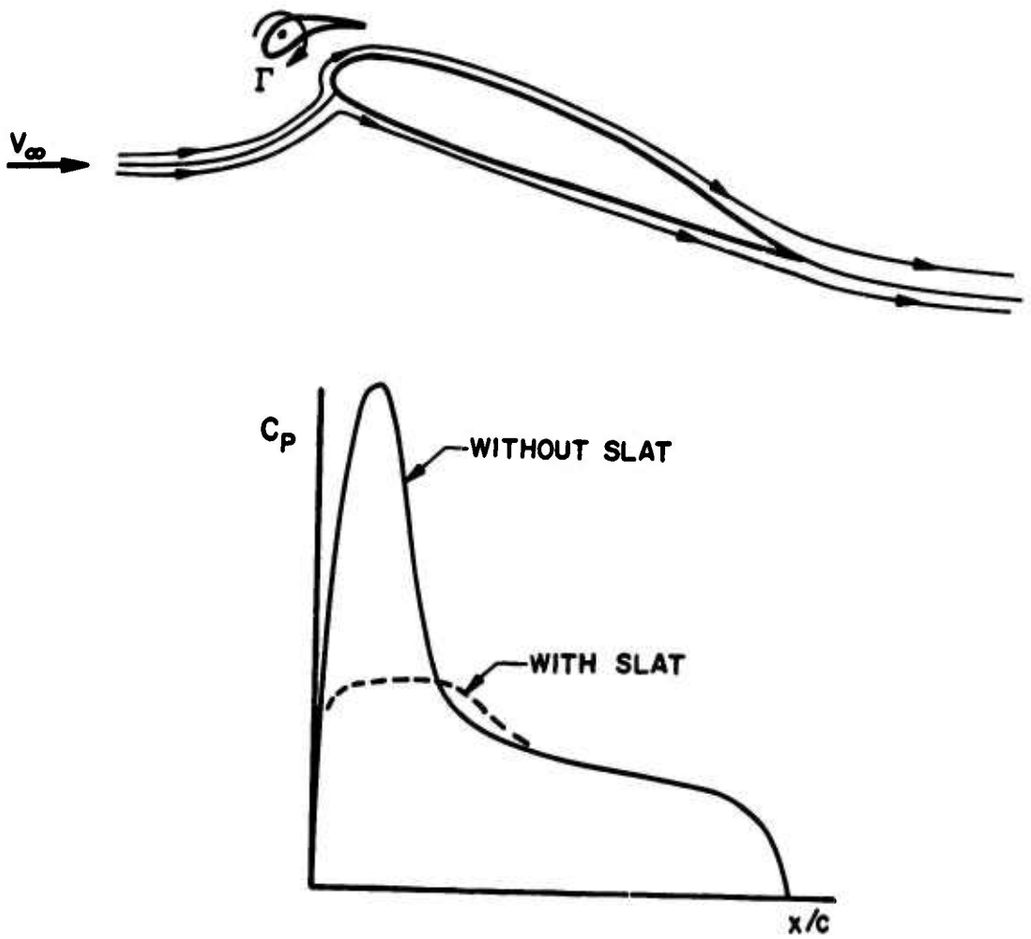

Figure 1.-A basic theoretical model of a leading edge slat.

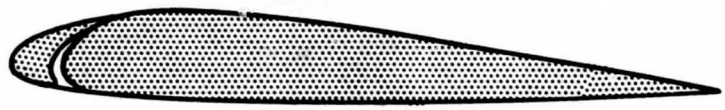

AIRFOIL GEOMETRY – SLAT RETRACTED

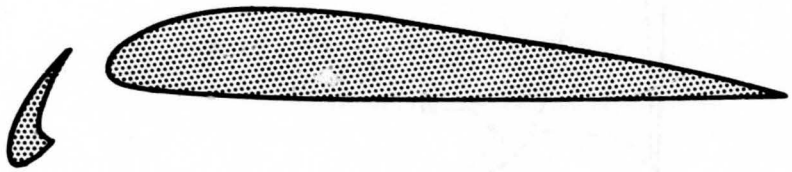

AIRFOIL GEOMETRY – SLAT EXTENDED

Figure 2.-Slat designed to retract to form main airfoil leading edge.

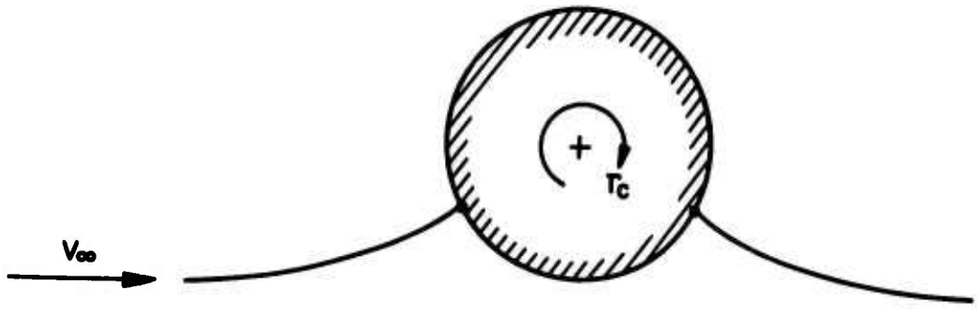

Figure 3.-Flow about a circular cylinder with circulation Γ_C.

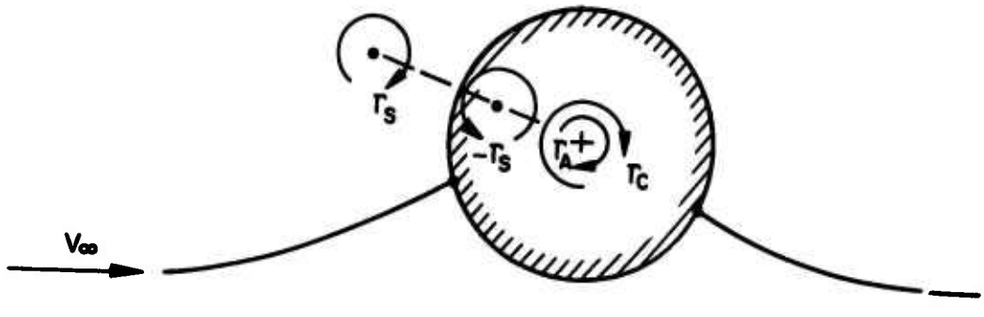

Figure 4.-Flow about the circular cylinder of figure 3 in the presence of an external point vortex Γ_S. The rear stagnation point is fixed.

GENERAL POLE DEFINED AIRFOIL - CIRCLE PLANE

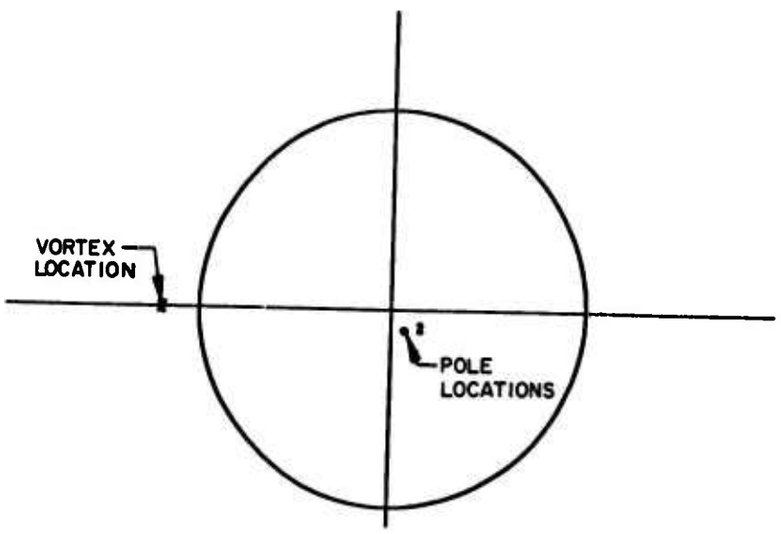

POLE DEFINITIONS CASE JK21

NO.	ORD	RADIUS	OMEGA	A	B
1	1	0.12	-50.0	1.0	0.0
2	2	0.12	-50.0	.07963454	-.0777418

VORTEX DEFINITIONS

	VALUE	DELTA
RADIUS	1.20	0.01
THETAV	180.0	0.0
DEL CL	0.0	0.005

Figure 5.-Circle plane used for defining pole airfoil and initial point vortex location and strength.

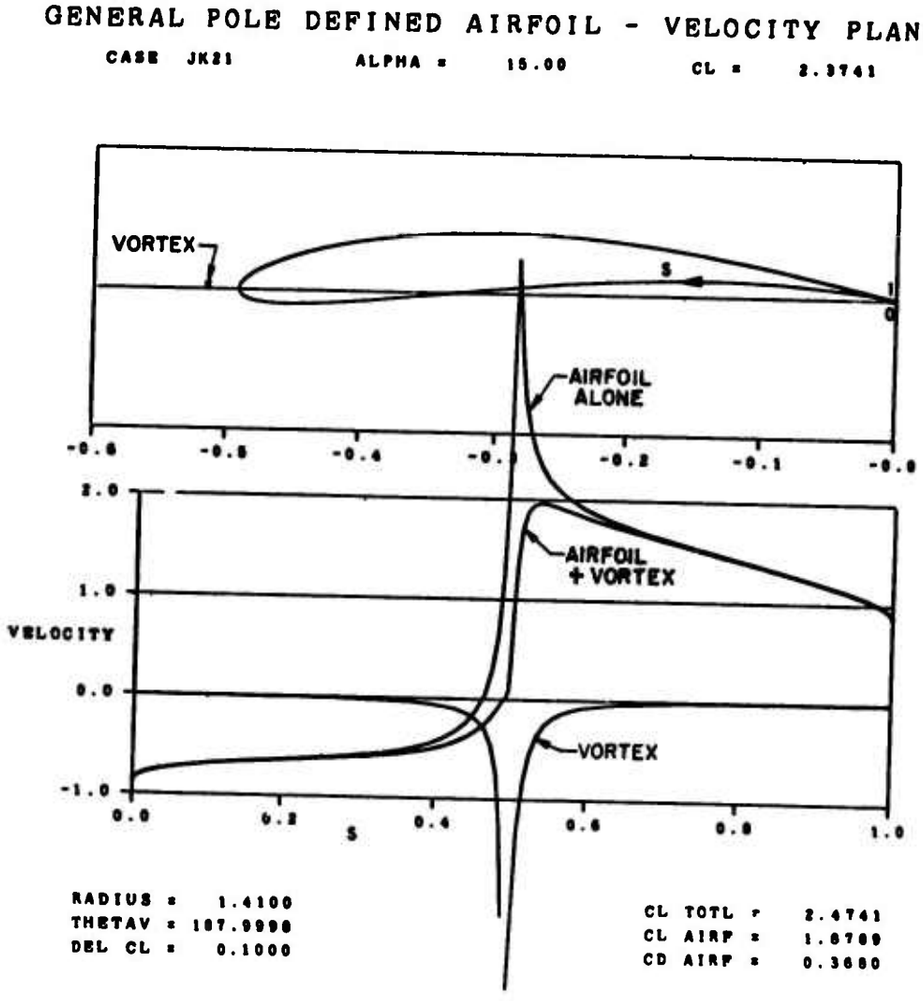

Figure 6.-Pole airfoil geometry and velocity distributions on airfoil alone and airfoil with vortex present. S is the arc length around the airfoil surface beginning at the lower surface trailing edge. The total airfoil perimeter equals one.

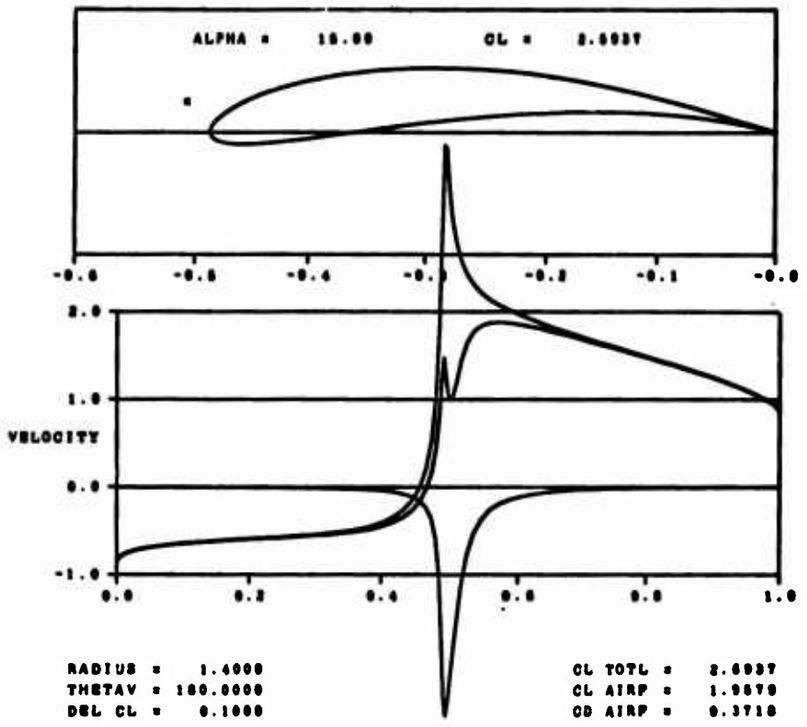

(a)

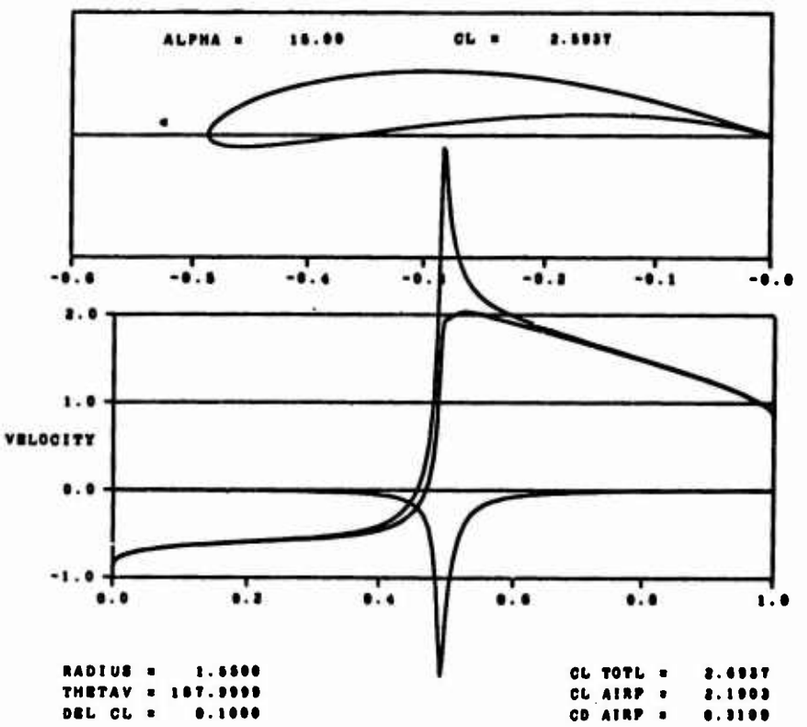

(b)

Figure 7.-Sample results showing spiked modulation distribution (a), and smoothed modulation (b) obtained by adjusting the vortex position.

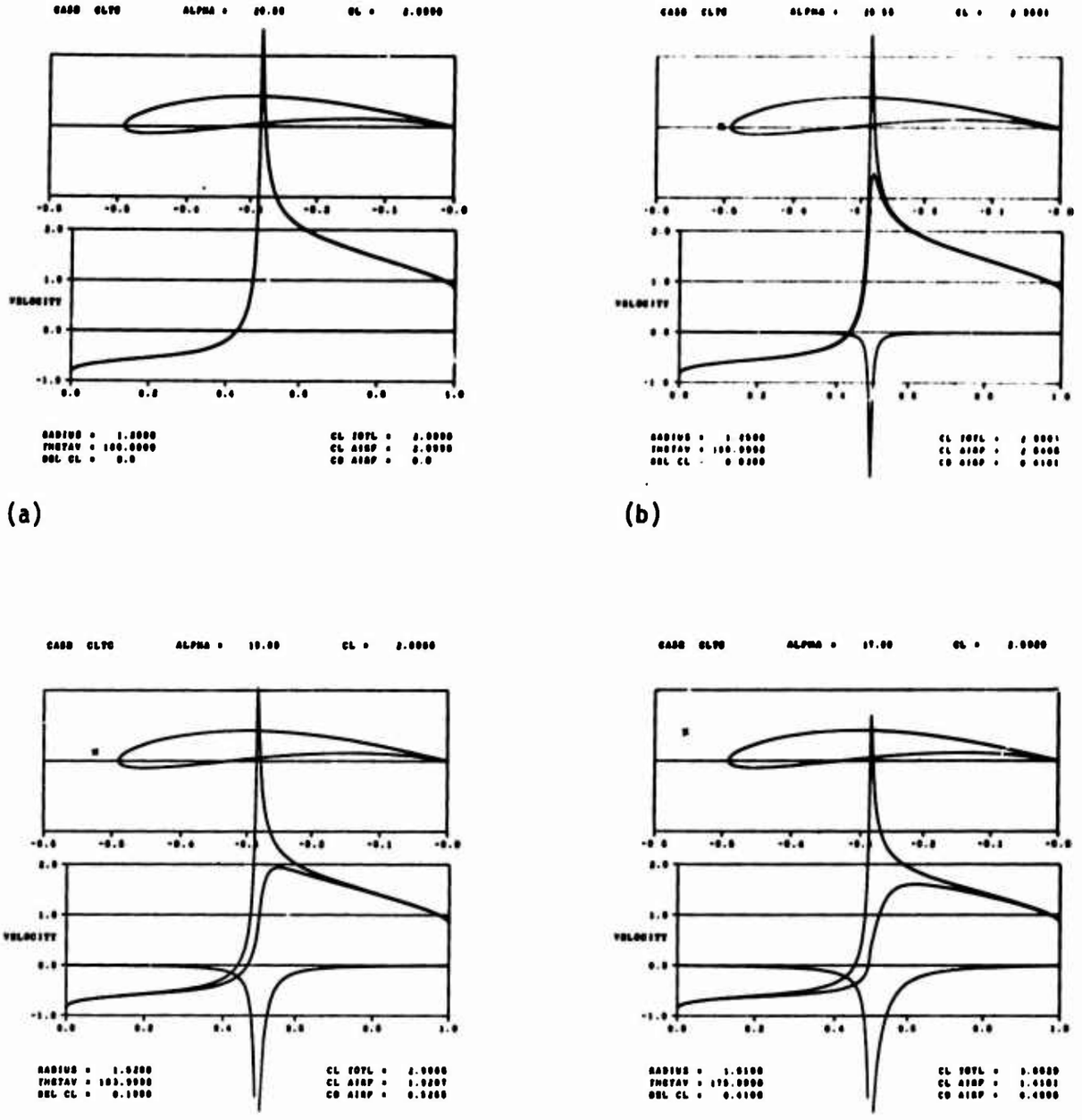

Figure 8.-Sample results for Example 1, C_{L_T} = 3.0. (a) α = 20.8°, no vortex, (b) α = 20.5°, C_{L_S} =0.335, (c) α = 19.0°, C_{L_S} = 1.097, and (d) α = 17.0°, C_{L_S} = 1.584.

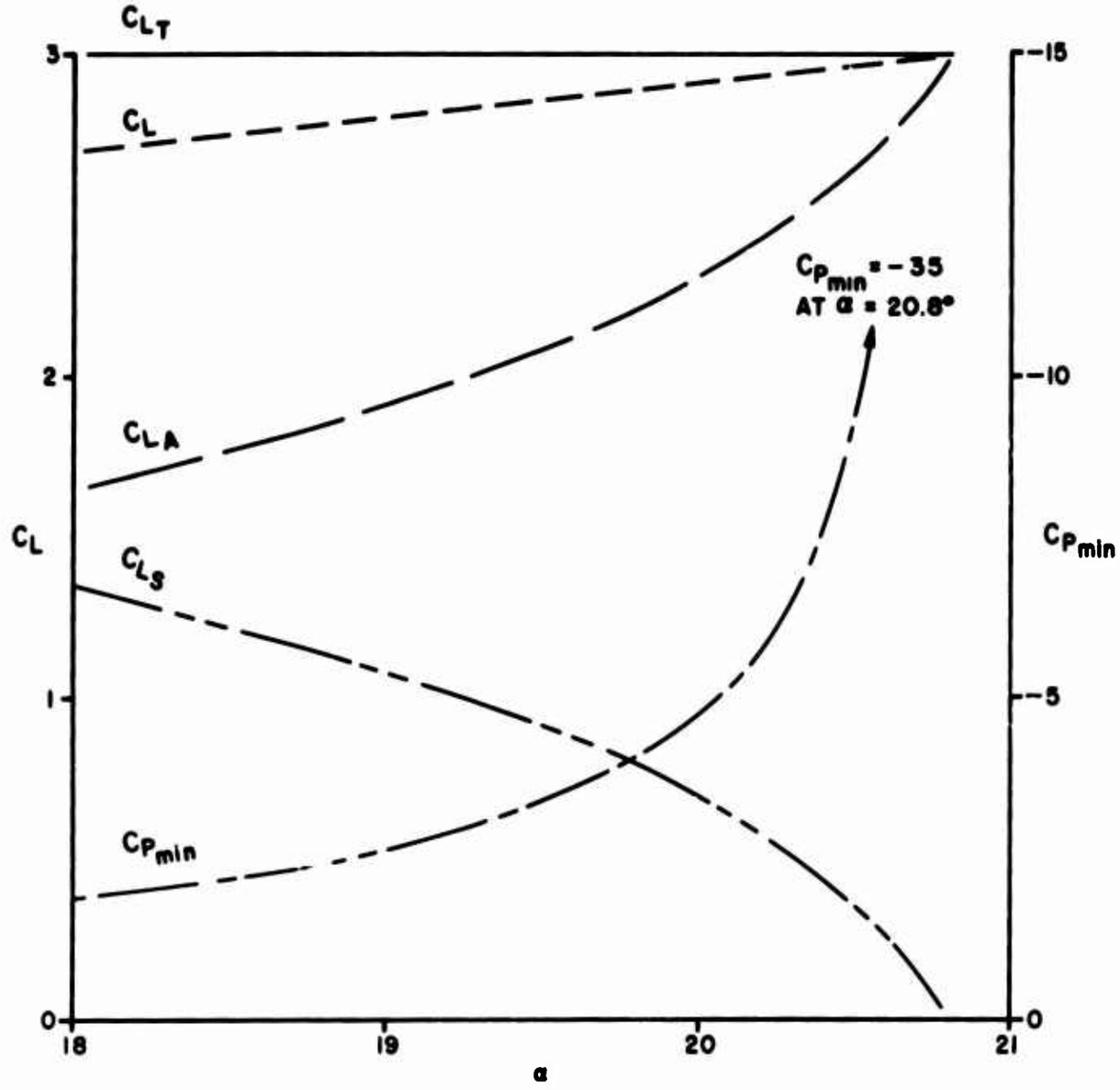

Figure 9.-Results for Example 1. Vortex strength and position adjusted to hold $C_{L_T} = 3.0$ as α is varied.

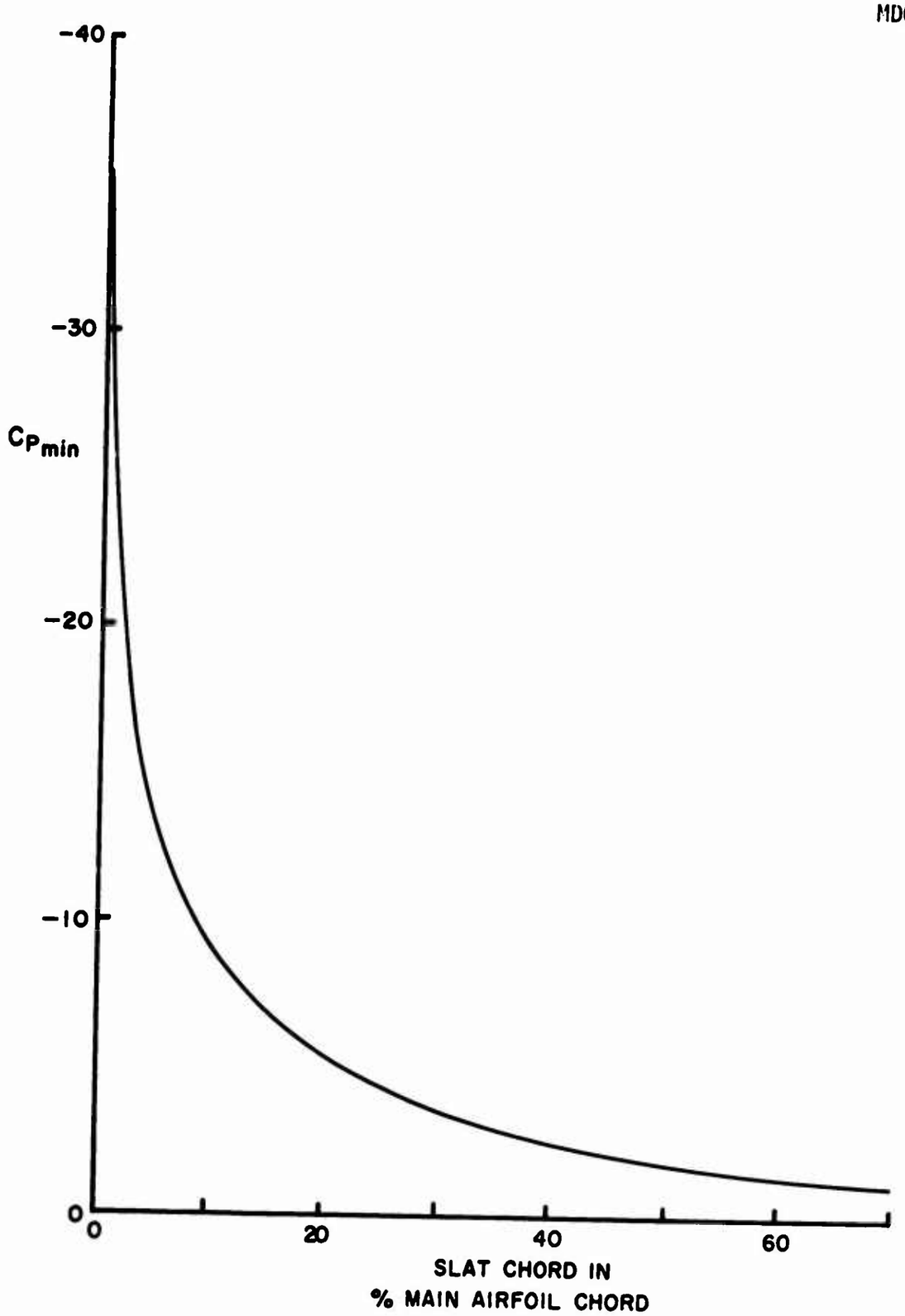

Figure 10.-Results for Example 1. $C_{P_{min}}$ versus implied slat chord required to obtain it. C_{L_T}= 3.0.

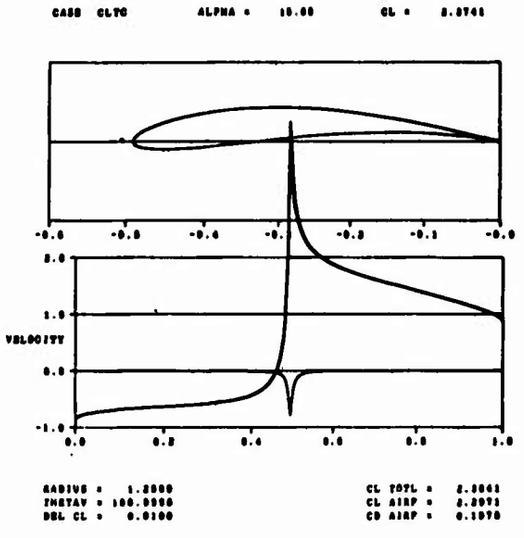

(a)

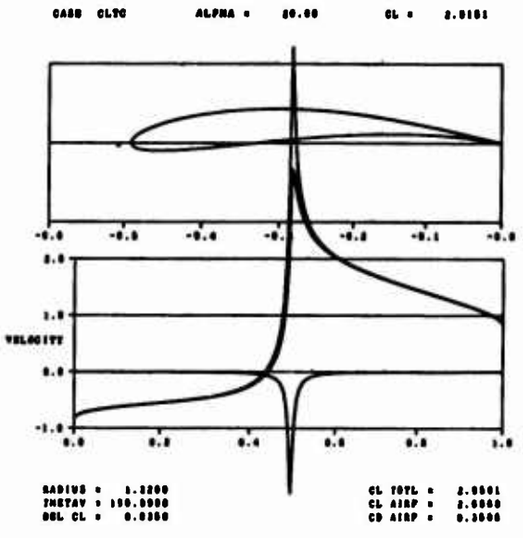

(b)

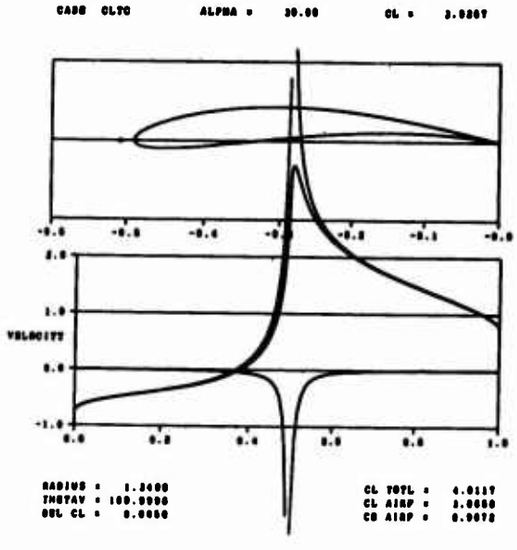

(c)

Figure 11.-Sample results for Example 2. Vortex strength and position adjusted to hold $C_{p_{min}} = -12$ constant as α is increased. (a) $\alpha = 15.0°$, (b) $\alpha = 20.0°$, and (c) $\alpha = 30.0°$.

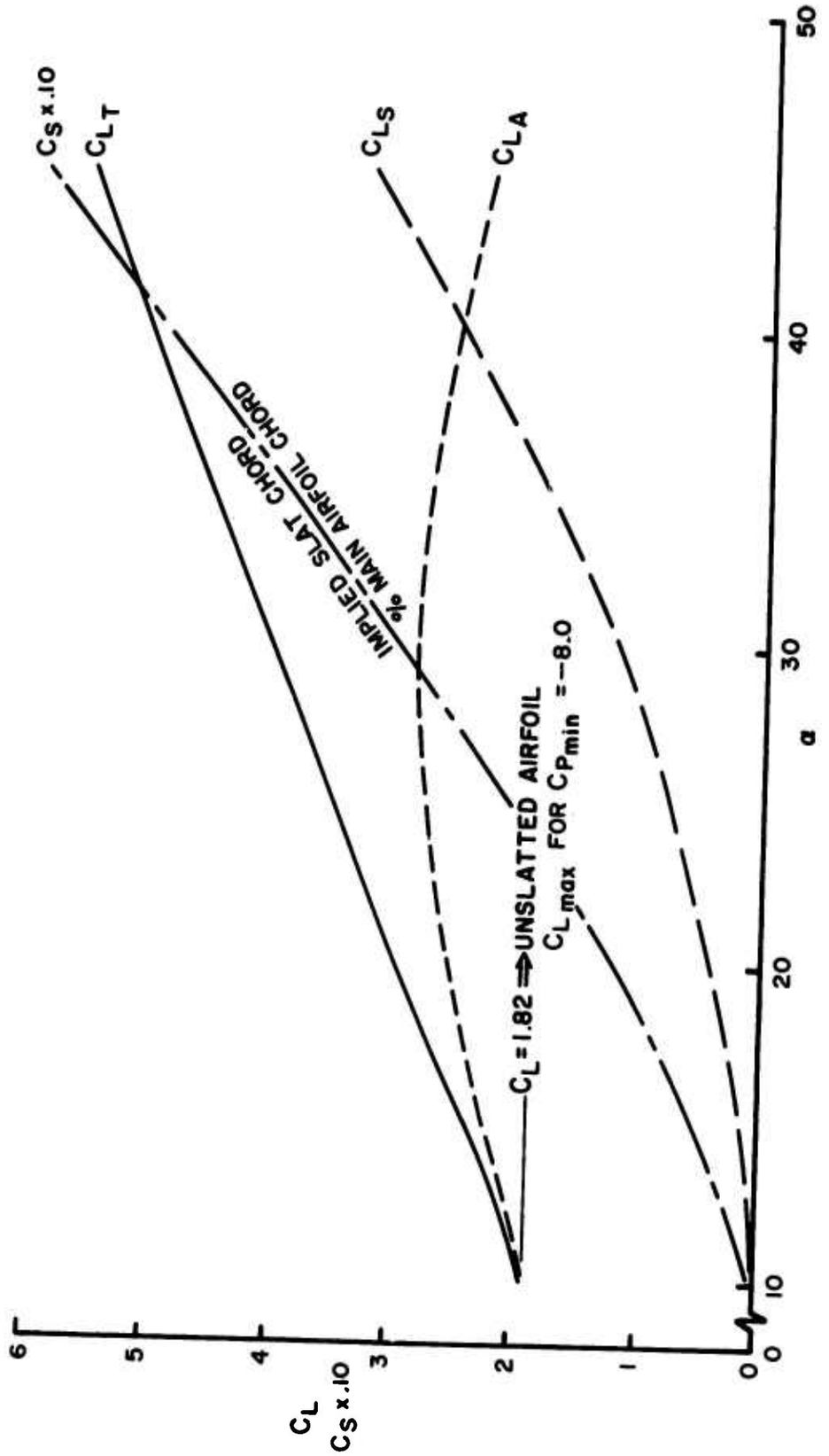

Figure 12.-Results for Example 2. Vortex strength and position adjusted to hold $C_{P_{min}} = -8.0$ constant as α is increased.

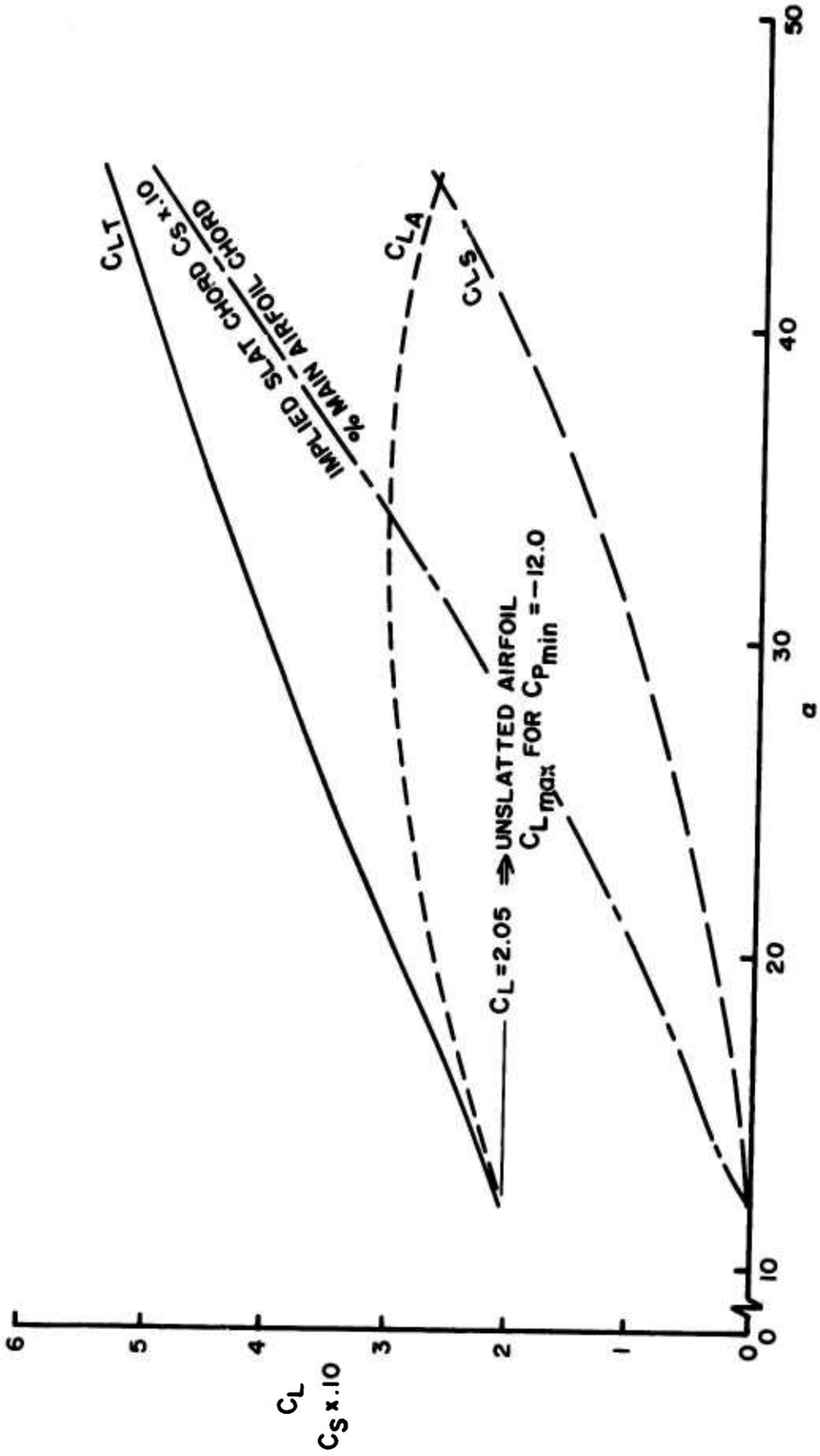

Figure 13.-Results for Example 2. Vortex strength and position adjusted to hold $C_{P_{min}}$ = -12.0 constant as α is increased.

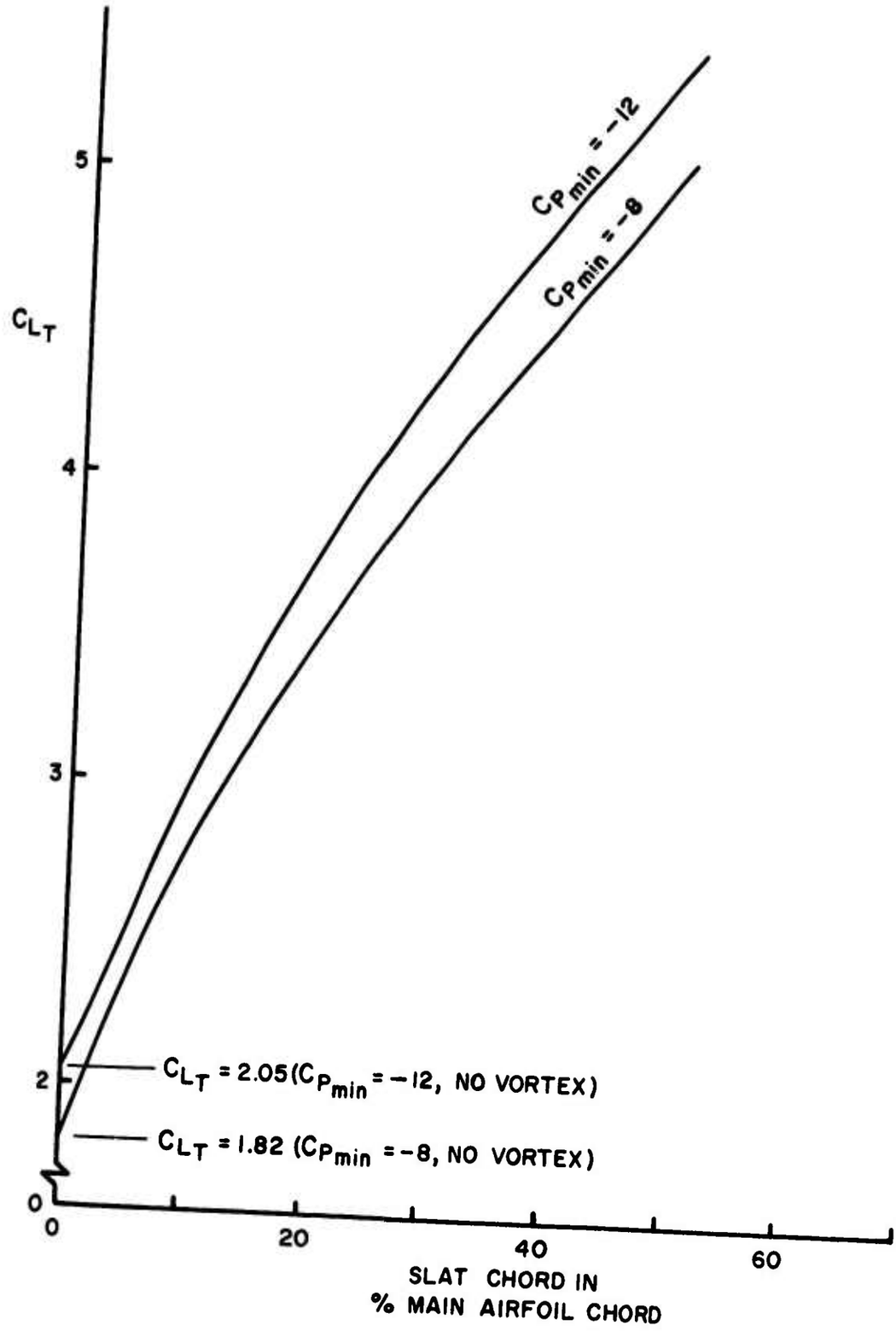

Figure 14.-Results for Example 2. Increase in C_{L_T} versus implied slat chord required to hold $C_{P_{min}}$ = -8, and -12.

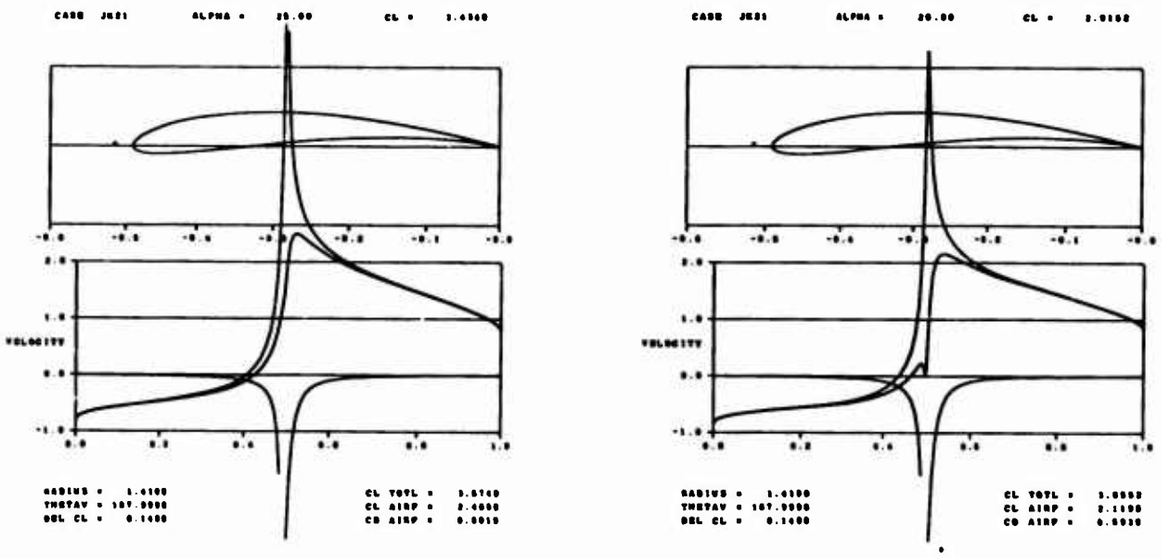

(a) (b)

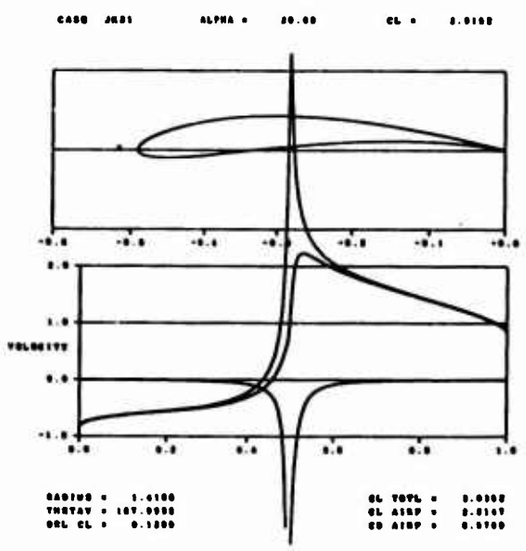

(c)

Figure 15.-Sample results for Example 3. (a) vortex strength and position set to obtain proper modulation at $\alpha = 25°$, (b) alpha reduced to 20° vortex same as (a), and (c) vortex strength adjusted to obtain proper modulation with vortex position the same as (a).

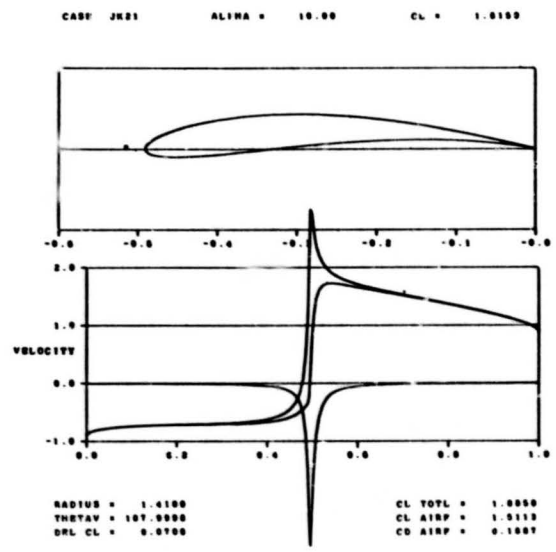

(a)

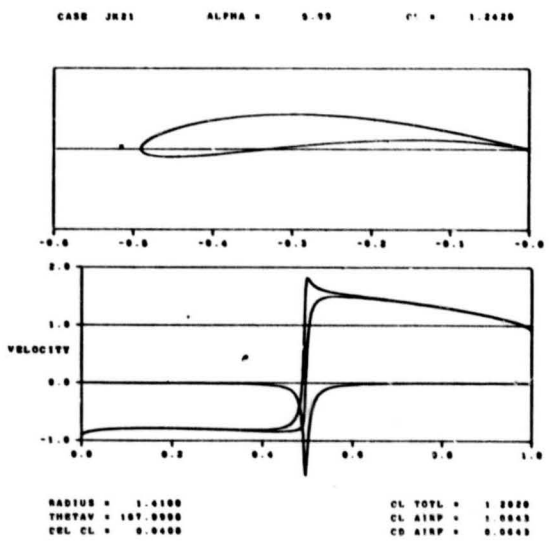

(b)

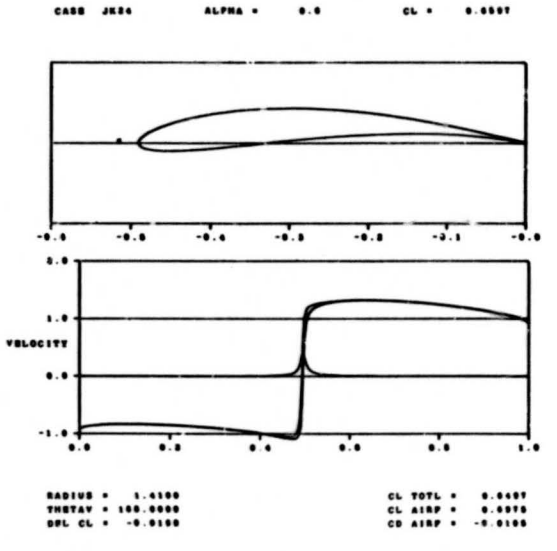

(c)

Figure 16.-Sample results for Example 3. Vortex position fixed at α =25°. Vortex strength adjusted to obtain proper modulation as α is reduced: (a) α = 10°, (b) α = 5°, and (c) α = 0°.

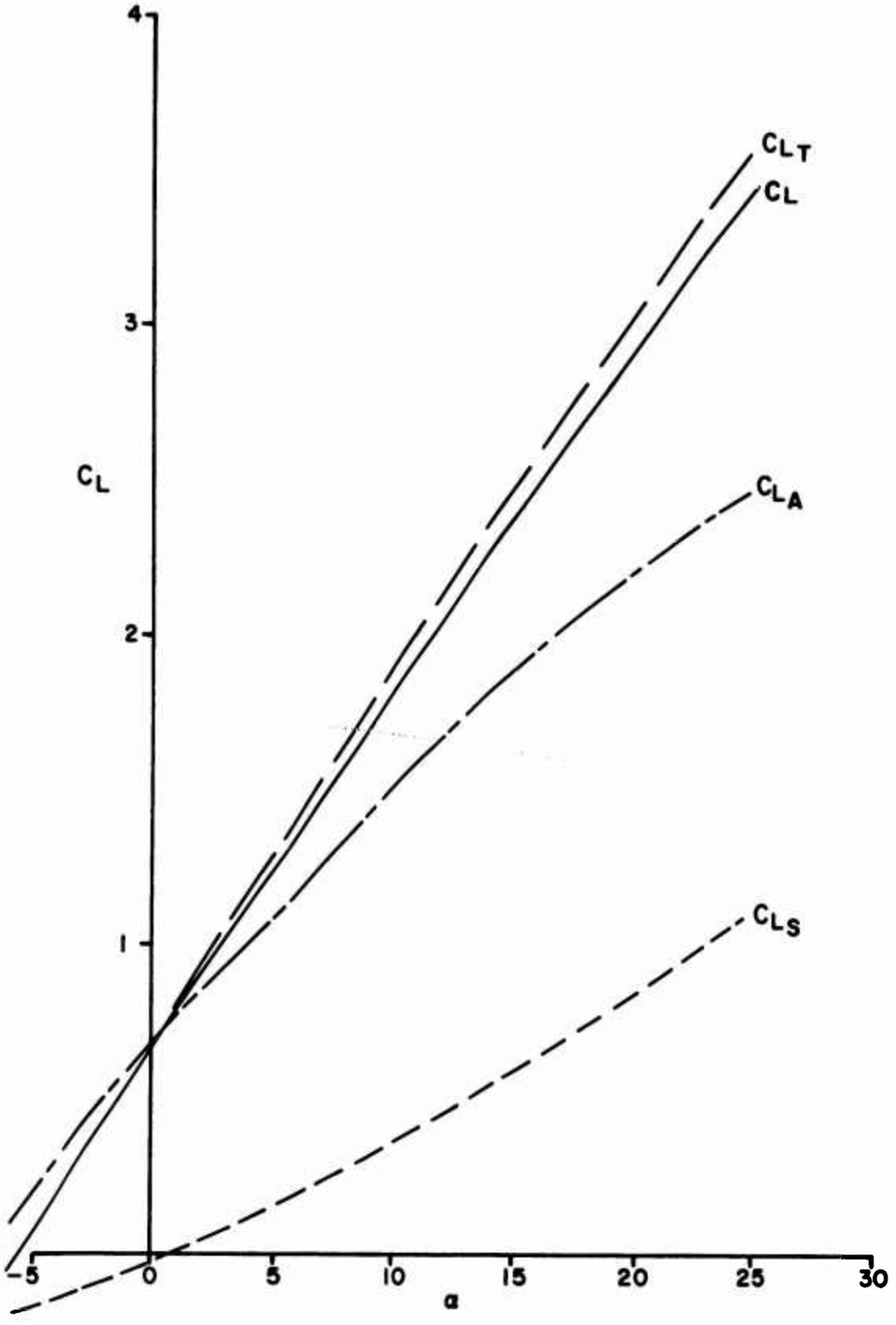

Figure 17.-Results for Example 3. Variation of lift coefficients with α, vortex position set at α = 25°, and vortex strength adjusted to obtain proper modulation at lower α's.

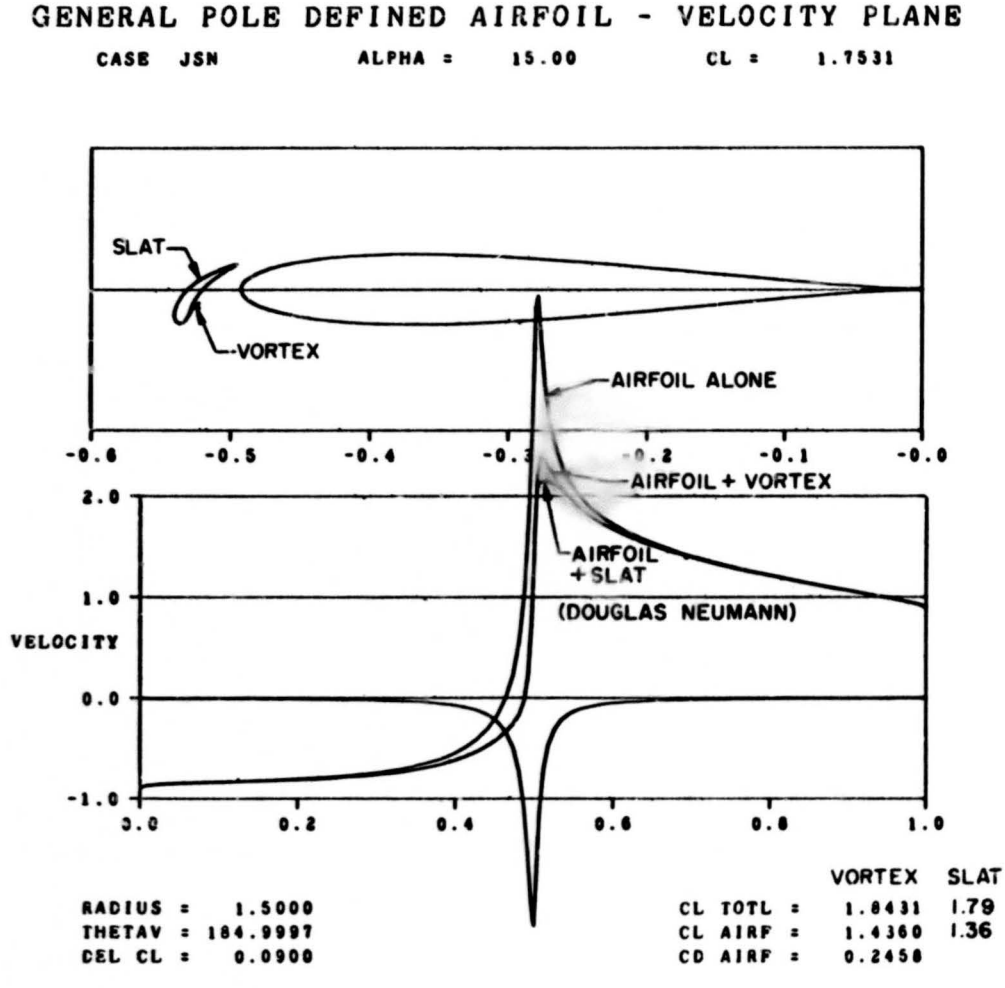

Figure 18.-Results for Example 4. Comparison of point vortex with a real slat using the Douglas Neumann potential flow program.

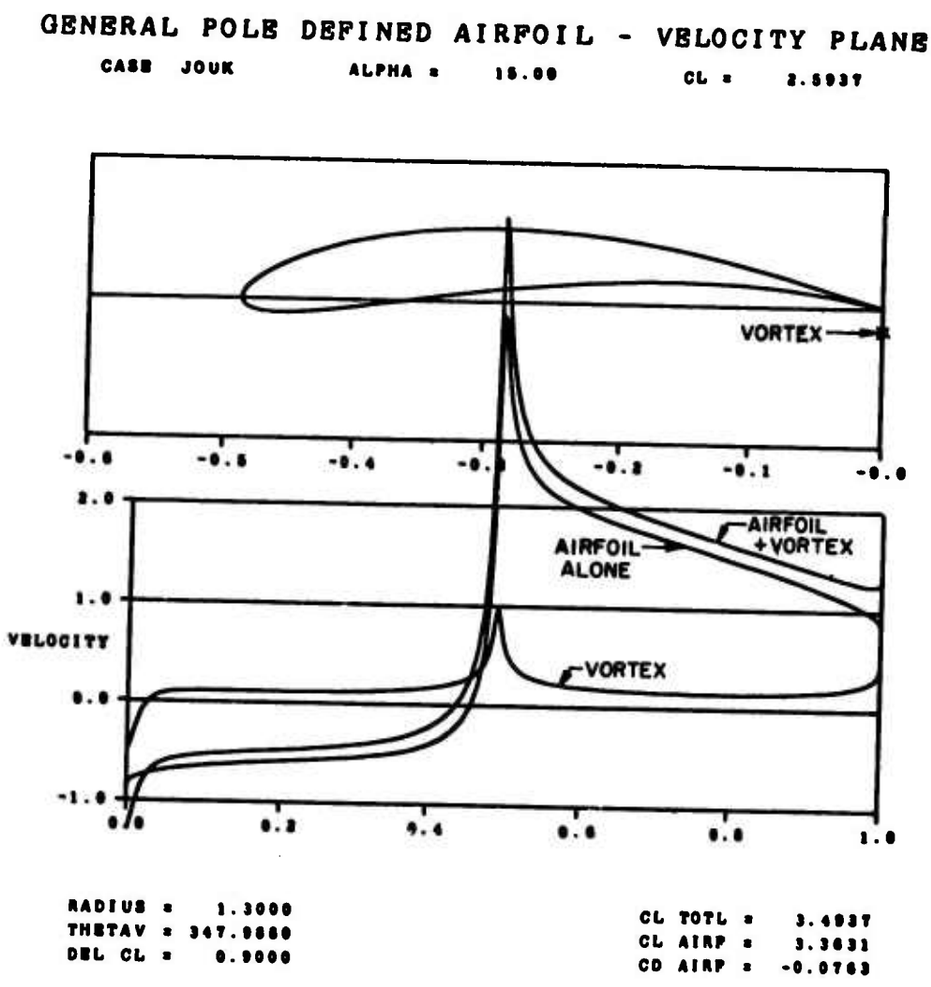

Figure 19.-Results for Example 5. Point vortex used to simulate a slotted flap.

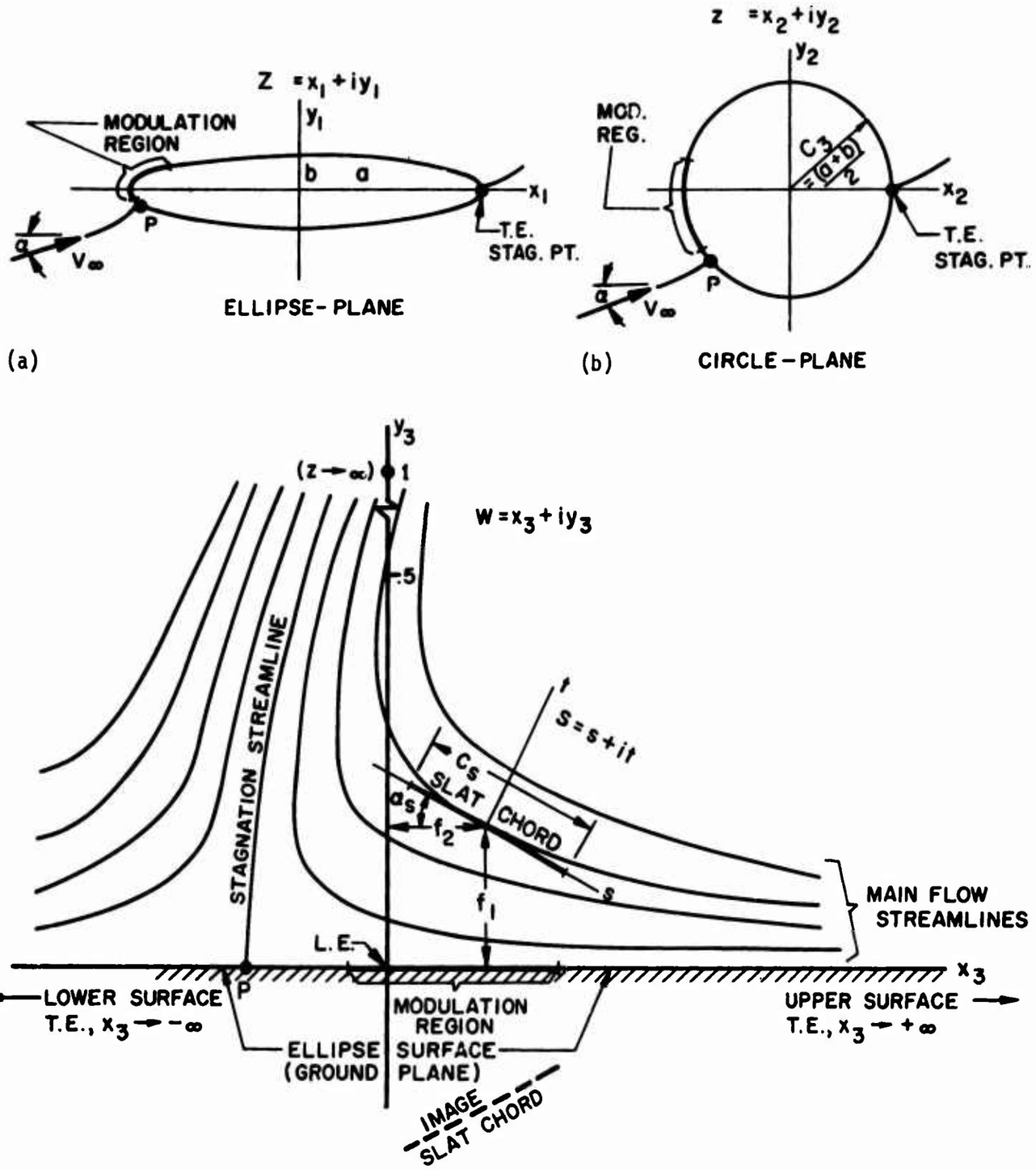

Figure 20.-Domains used in the distributed singularity analysis; (a) ellipse-plane, (b) circle-plane, and (c) half-plane. (Reference 3).

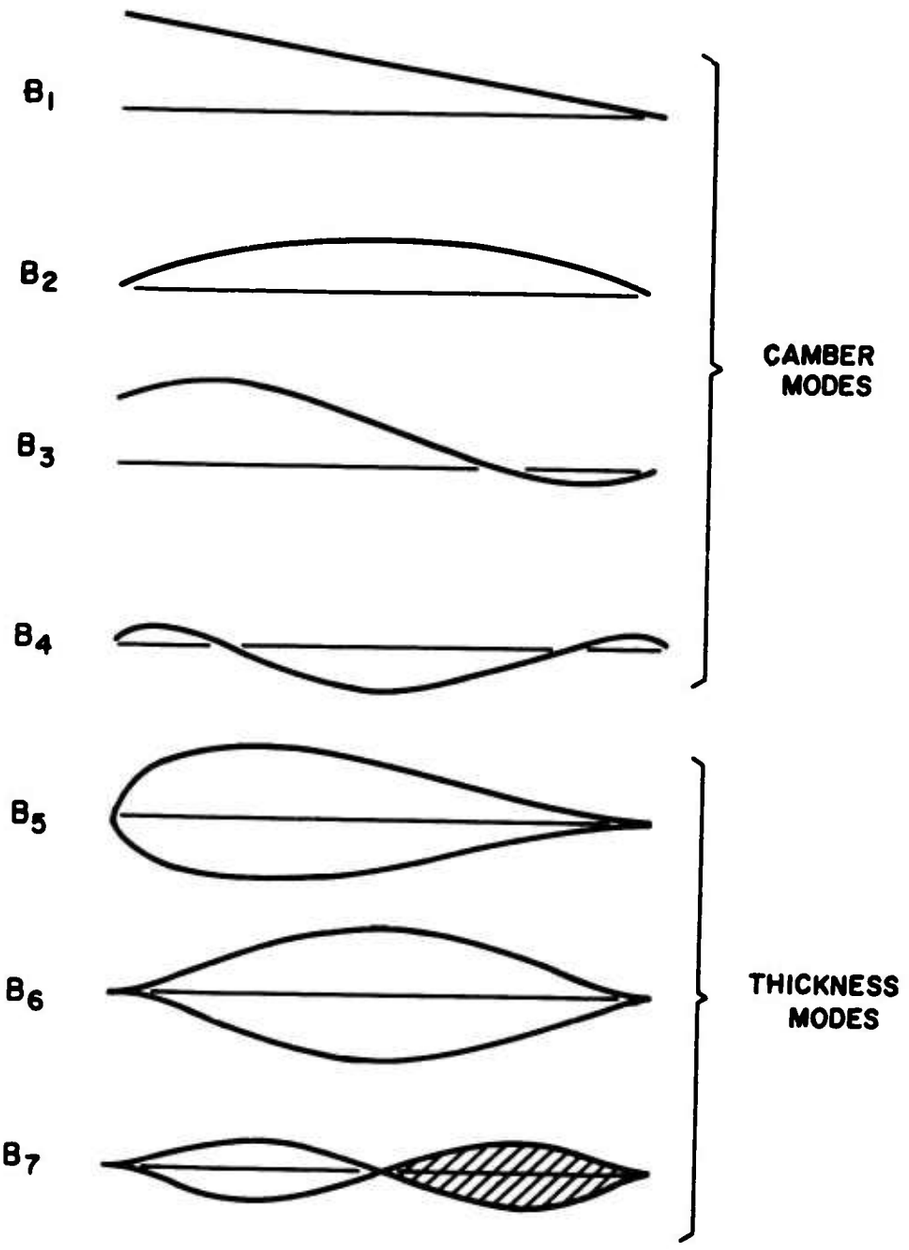

Figure 21.-Geometric mode shapes for uniform onset flow in the S-plane. (Reference 3).

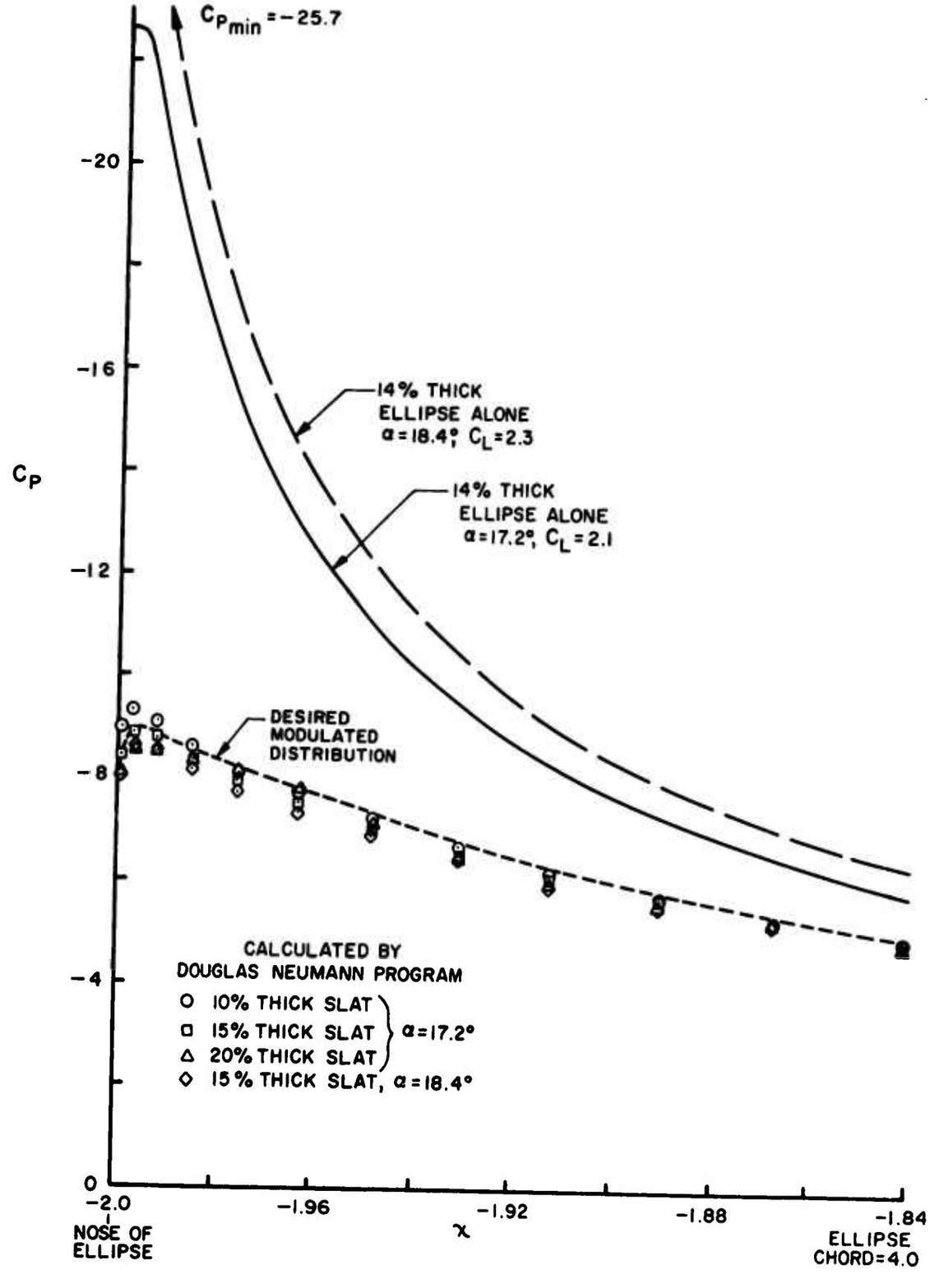

Figure 22.-Ellipse nose pressure modulation: desired modulated pressure distribution and that provided by the slats of figure 23.

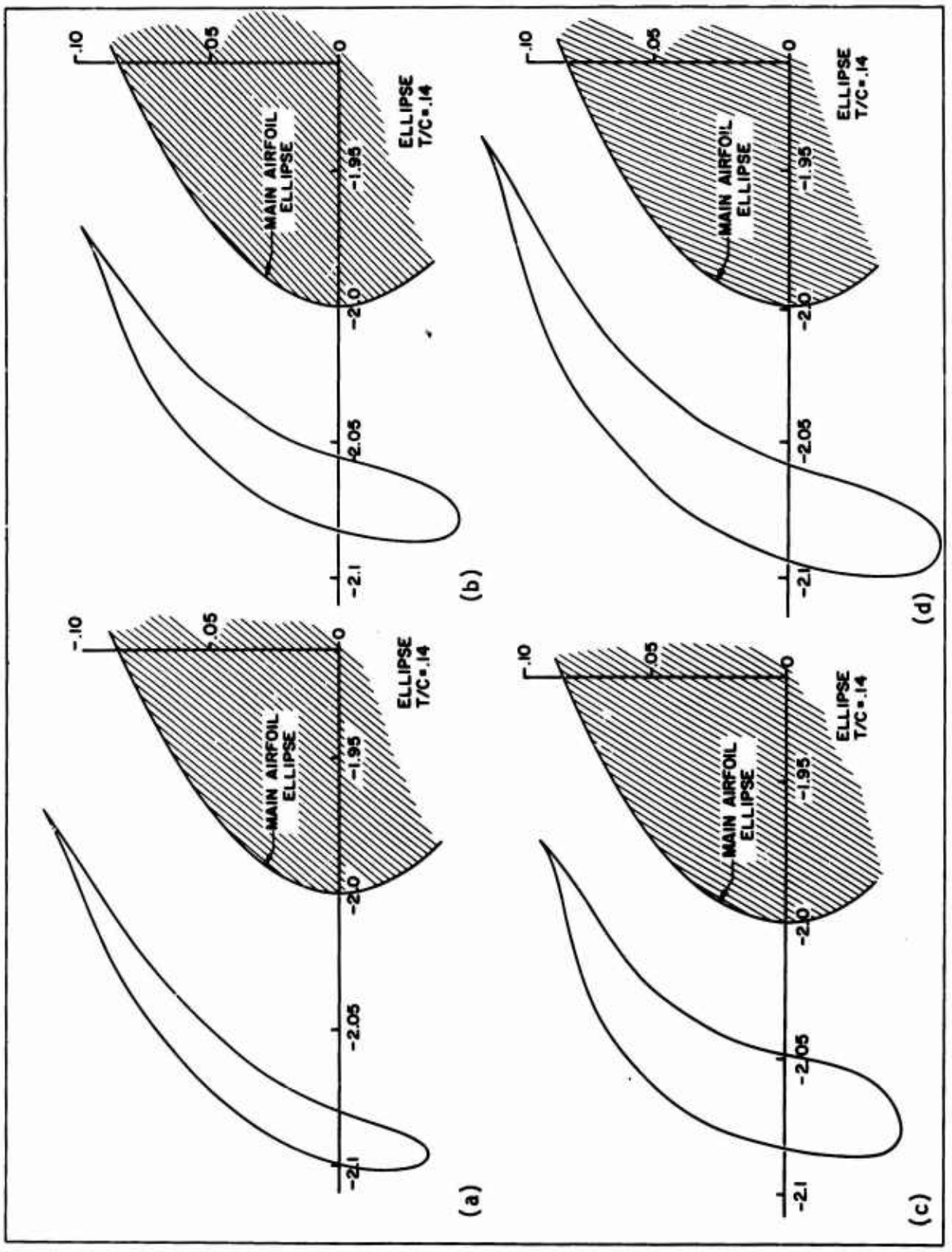

Figure 23.-Slats designed to provide the same modulation on the nose of the 14% thick ellipse. (a) 10% thick, $\alpha = 17.2°$, (b) 15% thick, $\alpha = 17.2°$, (c) 20% thick, $\alpha = 17.2°$, and (d) 15% thick, $\alpha = 18.4°$.